æ

18. RESOURCE ACQUISITION AND HOMEOSTASIS

25 December 2022

The most fundamental challenge of any organism is the acquisition of resources necessary for cell growth and replication, without which the transmission of genes to the next generation is impossible. Cells must also avoid predation, infection, and other sources of mortality, but this requires resource investment as well. The goal here is to consider some of the evolved strategies that single-celled organisms exploit to harvest nutrients, often with extremely low environmental concentrations.

Nutrient acquisition takes many forms, from the direct uptake of small molecules from the environment to the fixation of carbon by photosynthesis to the engulfment of smaller cells by phagocytosis to the scavenging of host nutrients by intracellular parasites. Rather than provide an encyclopedic coverage of the topic, only the first two of these strategies will be considered in detail here.

Although the molecular details can be quite complicated, relatively simple models can describe in mechanistic terms the basic responses of uptake rates to ambient nutrient concentrations. At the very least, these models highlight the key cellular features that need to be quantified to understand the basis for interspecies differences in nutrient-uptake parameters. Unfortunately, they also point to substantial gaps in our knowledge. Photosynthesis is of particular interest as it fuels the biological world, and yet has unexplained inefficiencies.

Finally, because all cellular machinery has optimal operating conditions, homeostatic mechanisms exist to keep internal physiological conditions (e.g., ion balance) relatively constant in the face of a variable external world. Such challenges impose a recurrent energy cost to the maintenance budget of all cells. A brief overview will be given for two key homeostatic mechanisms – osmoregulation and the maintenance of an internal physiological clock.

Adaptive Fine-tuning of Elemental Composition

As outlined in Chapter 7, ~ 20 elements are essential to the growth of most cells. The bulk of biomass consists of carbon, hydrogen, oxygen, nitrogen, phosphorus, and sulfur atoms (diminishing in that order), and to lesser extent the cations potassium, magnesium, calcium, and sodium, and ~ 10 trace metals. Different environments can provide quite different blends of these elements, and this can promote the growth of some species over others, depending on their elemental requirements and uptake efficiencies (Tilman 1982).

Motivated by the fact that the basic building blocks of life vary in elemental

content (C, N, P, and S in particular), several authors have suggested that natural selection fine tunes the elemental composition of cells to prevailing environmental conditions through genome-wide shifts in the use of alternative nucleotides and/or amino acids. Under this view, organisms living in environments depleted for one of these elements are expected to evolve towards reduced reliance on the same element in their building-block repertoires over eons of time. For the same reason, enzymes involved in the metabolism of a scarce element are expected to have nucleotides and/or amino acids depleted for the same element (Baudouin-Cornu et al. 2001; Alves and Savageau 2005; Acquisti et al. 2009; Grzymski and Dussaq 2012; Fasani and Savageau 2014). It has even been suggested that the genetic code is structured in such a way that the nitrogen content of the nucleotides within codons is correlated with that of the encoded amino acids, generating a reinforcing effect at the level of nucleotides and amino acids (Bragg and Hyder 2004; Shenhav and Zeevi 2020).

Consistent with this view, Baudouin-Cornu et al. (2001) found that enzymes involved in the assimilation of sulfur and carbon in *E. coli* and *S. cerevisiae* contain amino acids that are, respectively, depleted with sulfur and carbon (e.g., methionine and cysteine in the case of sulfur). Similar claims have been made based on the absence of methionine and cysteine residues in cyanobacterial proteins with enhanced expression during times of sulfur depletion (Mazel and Marliére 1989), and on the differential utilization of nitrogen in proteins involved in anabolism vs. catabolism (Acquisti et al. 2009). On the other hand, Baudouin-Cornu et al. (2001) found no such depletion for sulfur metabolizing enzymes in mammals, arguing that this is because mammals are less deprived of sulfur.

Underlying these causal arguments are two strong and often unstated assumptions: 1) that the genomic attributes of extant species have been molded evolutionarily by the current features of the environments that they inhabit; and 2) that natural selection is capable of promoting incremental modifications at the codon level. The first assumption ignores the possibility that matching between genomic requirements and the environment may be a simple consequence of competitive assortment of species, with differences in the former having evolved for entirely different reasons. The second assumption relies on the idea that natural selection is powerful enough to discriminate among alternative building blocks differing in just one or two atoms of a particular type. The matter of whether the population-genetic conditions necessary for such selection are likely to be met can be evaluated by applying the same strategy outlined in Chapter 17 for the differential costs of amino acids, but in this case by measuring costs in units of elemental composition rather than ATP equivalents.

Consider first the selective usage of alternative nucleotides on the basis of their carbon and nitrogen contents. Shenhav and Zeevi (2020) suggested that the vertical distribution of the C:N ratio in marine environments has driven the evolutionary divergence of genome-wide nucleotide usage in the bacteria inhabiting different depth strata. To determine whether the strength of selection required for such genome-wide remodeling is feasible, consider that over a range of growth conditions, the dry weight of *E. coli* and other bacterial cells consists of 45 to 47% carbon and 10 to 13% nitrogen (Folsom and Carlson 2015; Chapter 7). The dry weight of an average cell in this species is ~ 0.00038 ng, which given the molecular weights of C and N, implies $\sim 9 \times 10^9$ C and $\sim 2 \times 10^9$ N atoms per cell. An A:T nucleotide pair in DNA

contains 10 C and 7 N atoms, whereas a G:C pair contains 9 and 8, respectively. Thus, exchanges between A:T and G:C pair add/subtract just a single atom of each of these elements, changing the fractional elemental usages of C and N per cell by $\sim 10^{-10}$ and 0.5×10^{-9}, respectively.

Given that no known species has an effective population size of $N_e > 10^{10}$, such a single genomic base-pair shift in a nontranscribed genomic region is expected to be barely detectable by natural selection, if at all. However, as most genes are represented by multiple copies of mRNA per cell, these numbers need to be multiplied accordingly for transcribed genes. Nonetheless, because the average number of mRNA copies per cell per gene is < 10 in *E. coli* (Chapter 3), and unlike DNA, mRNAs are single-stranded, this still leaves the elemental cost very close to, if not below, the drift barrier. Thus, it appears doubtful that nucleotide usage can be selected on the basis of C:N composition.

Now consider the situation at the amino-acid level. The maximum difference in carbon-atom content among the 20 amino acids is 9 (tryptophan vs. glycine) and for N is 3 (arginine vs. several other residues). The maximum fractional impact of a single amino-acid substitution is then $\sim 10^{-9}$ for both C and N for a gene with just a single protein copy per cell for *E. coli.* However, for *E. coli,* the mean number of proteins per cell per expressed gene is $\simeq 2000$, with a very large standard deviation ($\simeq 5000$) (Lynch and Marinov 2015). As this will frequently place the maximum fractional impact in the range of 10^{-6} to 10^{-5}, this suggests that the elemental costs of some amino-acid substitutions are in the realm of being detectable by natural selection, at least in bacteria.

The conditions necessary for effective selection on elemental composition are less conducive in eukaryotes. Because the average number of proteins per gene per cell increases less than linearly with cell volume (with the $\sim 2/3$ power; Chapter 7), the cost/benefit of an amino-acid substitution is expected to decline with cell volume. Thus, because N_e declines by two to five orders of magnitude from bacteria to eukaryotes, and cell volume increases by one to three orders of magnitude, it is questionable as to whether cellular elemental composition can be driven by natural selection in eukaryotes, especially in multicellular species with large cells. This provides a simple alternative explanation for the mammalian results noted above.

In summary, despite the strong arguments that have been made for the global significance of selection on elemental composition, even extending to the evolution of the genetic code (see Rozhoňová and Payne (2021) and Xu and Zhang (2021) for compelling counterpoints), it is striking that all such studies are devoid of formal evolutionary analyses, despite their relatively straight-forward utility. Notably, in one of the only applications of this kind, Günther et al. (2013) found that high-frequency derived alleles in *Arabidopsis* populations have elevated nitrogen content, contrary to expectations for a plant expected to be under nitrogen limitation.

Given the tiny selective pressures involved and the extremely long time time scales required for genome-wide repatterning of elemental composition, to the extent that matchings in organismal and environmental features occur, a more likely explanation is that other evolutionary forces drive cellular elemental composition, with species then assorting into environments that are most compatible with elemental demands. One such force is mutational bias, which plays a strong role in guiding nucleotide content of genomes across the Tree of Life, often operating in

a direction contrary to that of natural selection (Long et al. 2017). Future work in this area would profit from a more holistic conceptual approach incorporating general evolutionary principles.

Nutrient Uptake Kinetics

Nutrient uptake rates are concentration-dependent. At low substrate concentrations, consumers are limited by resource encounter rates, whereas at high concentrations, uptake mechanisms become saturated. One of the simplest models for nutrient-uptake kinetics captures both of these effects, and has the Michaelis-Menten form (identical in structure to the Monod growth equation introduced in Chapter 9, and derived for more general enzyme kinetics in Chapter 19),

$$V = \frac{V_{\max} S}{k_S + S}, \tag{18.1}$$

where V is the rate of uptake of the nutrient (substrate) with concentration S, and k_S is the concentration at which V is 50% of it maximum value, $V_{\max}$. Written in this way, the rate of nutrient is a hyperbolic function of the substrate concentration, which closely approximates empirical results from hundreds of studies. The ratio $V_{\max}/k_S$ is close to the uptake rate per unit nutrient for $S \ll k_S$ and is commonly referred to as the uptake affinity.

The model parameters $V_{\max}$ and k_S are simple summary descriptors of potentially complex cellular mechanisms, leaving unexplained the actual determinants of such patterns. A more mechanistic model (Foundations 18.1) directly accounts for random encounter rates of the substrate by molecular diffusion and active transport across the cell membrane, while retaining the hyperbolic form of Equation 18.1 .

Substantial attention has been given to nutrient-uptake parameters in phytoplankton species, particularly for nitrogen and phosphorus, which commonly limit growth in freshwater and marine ecosystems. The key parameters appear to be cell-volume dependent. Summarizing over a wide phylogenetic range of species, Edwards et al. (2012) found power-law exponents of 0.82 and 0.94 for $V_{\max}$ (per cell) for N and P uptake, respectively, when scaled against cell volume, and exponents of 0.33 and 0.53 for k_S for these same elements. Uptake affinities ($V_{\max}/k_S$) for both elements also increase with cell size, with allometric scaling powers on the order of 0.75 to 0.85. Similar results were obtained by Lomas et al. (2014) and Marañón (2015). Note, however, that although uptake affinities have positive allometric coefficients, implying that larger cells (on average) have higher rates of nutrient uptake on a per-cell basis, because the coefficients are < 1.0, on a per-biomass basis, uptake rates actually decline with increasing cell size.

What are the underlying determinants of these scaling features? In Foundations 18.1, it is shown that $V_{\max}$ is equivalent to the product of the number of transporters on the cell surface (per cell) and the rate of handling of substrate molecules by an engaged transporter. As the surface area of a cell is proportional to the square of the linear dimension, whereas cell volume is proportional to the cube of the latter, if the density of transporters per unit surface area remains constant, one would

expect $V_{\max}$ to scale with the 2/3 power of cell volume (with variation around this expectation owing to shape differences). Some suggestion that such scaling occurs derives from observations on uptake rates for several amino acids in a polyploid series of yeast cells (from haploidy to tetraploidy) that increase in cell volume but are otherwise isogenic (Hennaut et al. 1970). However, the fact that the exponents of $V_{\max}$ and $V_{\max}/k_S$ (0.82 to 0.94, noted above) for interspecific comparisons are substantially higher than 0.67 suggests an increase in transporter density and/or a decrease in handling time with cell volume.

The half-saturation constant k_S is also expected to increase with transporter numbers and rate of handling (Foundations 18.1), albeit in a somewhat different way, so a positive scaling of this parameter with cell volume is again expected. Why the allometric scaling of k_S (noted above) is reduced two-fold relative to that for $V_{\max}$ is unclear, but this could happen if the capture rates of transporters declined with increasing cell volume. In principle, the theory in Foundations 18.1 might be brought in closer alignment with empirical observations by directly evaluating the relationship between transporter number and the geometric features of cells, but the necessary empirical work remains to be done.

There has been considerable speculation on the adaptive designs of various sized cells for particular environments (e.g., Chakraborty 2017), with Litchman et al. (2007) arguing that the uptake kinetics of various phytoplankton groups were essentially permanently molded by the physical/chemical environments in which the groups emerged phylogenetically, generally hundreds of millions of years ago. However, this frozen-phenotype view belies the rapidity with which metabolic processes can evolve in microbes (Helling et al. 1987; Maharjan et al. 2007; Blount et al. 2012; Samani and Bell 2016). As noted above for nucleotide and amino-acid composition, a more likely explanation for any phenotype-environment matching is simple competitive assortment in temporally and spatially varying environments.

Channels and transporters. Lipid membranes are essentially impermeable to the kinds of ions and organic molecules that cells harvest and export for nutritional and homeostatic reasons. Thus, for nearly every type of essential molecule, specialized trans-membrane proteins are dedicated to selective transmission across the lipid bilayer. Relative to cytoplasmic proteins, such molecules can be viewed as being inside-out, in the sense that the exterior of the transmembrane domain is hydrophobic (to enable embedding into the lipid environment), whereas the channel interior is hydrophilic.

Membrane pores can be roughly partitioned into two categories. Channels are selective, sometimes gated, sieves that allow the transmission of specific molecules, while excluding others. As channels do not bind molecules directly, their ion transfer can approach the rate of diffusion. In contrast, transporters bind cargo directly, and that reduces rates of molecular transmission to levels in the range of 50 to 250 molecules per second, although most of the data are restricted to *E. coli* (Waygood and Steeves 1980; Naftalin et al. 2007) and yeast (Kruckeberg et al. 1999; Ye et al. 2001). Whereas channels operate in a passive manner and can only transport solutes down a concentration gradient, traffic through transporters requires energy to induce the structural changes necessary for opening and closing the pores on opposite sides of the membrane.

Cellular investments in membrane proteins are enormous. Approximately ~ 20 to 35% of genes in prokaryotes and eukaryotes encoding for them (Wallin and von Heijne 1998; Stevens and Arkin 2000), and they typically comprise on the order of 25% of the total protein mass in cells (Itzhak et al. 2016), and up to 50% of membrane surface areas (Chapter 17). Because many types of channels are found across the Tree of Life (Greganova et al. 2013), e.g., potassium channels (Loukin et al. 2005), and aquaporins (Abascal et al. 2014), they must have originated very early (pre-LUCA). On the other hand, many channel types have been lost from specific lineages but dramatically expanded in others. For example, potassium channels are absent from fission yeast, and only present as one copy in budding yeast, but have expanded to ~ 300 copies in *Paramecium.* Losses of transporters are particularly common in parasite lineages, which can, for example, obtain nitrogen-containing amino acids and nucleotides from their host cells, eliminating the need to import ammonia for biosynthesis.

How difficult is it to evolve membrane-embedded proteins? Although hydrophobic transmembrane domains are a key requirement for reliable membrane insertion, the barrier to such a condition may not be great. For example, numerous studies have found that small random peptides often spontaneously develop into α-helices that adhere to the surfaces of lipid bilayers and under some conditions even insert as bundles of several helices (Lear et al. 1988; Pohorille et al. 2005; Mulkidjanian et al. 2009). Part of the reason for the enhanced stability of α-helices when aligned along membranes is the partial sheltering of their hydrogen bonds from open water. Thus, for biophysical reasons alone, proto-channels may have been quite feasible in the earliest stages of cellular evolution.

There are many ways by which membrane pores use energy to drive the membrane passage of substrates. Many transporters couple the power from downhill diffusion of one molecule to the uphill work required for the import of a second molecule. Others cotransport protons or sodium ions (by the proton/sodium motive force) to drive cargo import. ABC (ATP binding cassette) transporters, found throughout bacteria and eukaryotes, utilize the energy from ATP hydrolysis to pump substrates against a concentration gradient. The exact number of ATP hydrolyses per substrate molecule is not firmly established, although it is thought to be near two, the same as the number of ATP-binding domains per transporter (Higgins 1992; Stefan et al. 2020). Some evidence suggests that transporters have ATPase activity even in the absence of substrate, leading to up to dozens of ATP hydrolyses per substrate-molecule uptake (Bock et al. 2019). Bacteria can also produce solute-binding proteins (SBPs) that sequester substrate molecules and then pass them on to cognate transporters (Driessen et al. 2000). In Gram-negative bacteria (with two membranes), the SBPs float freely in the periplasm, whereas in Gram-positives they are anchored to the cell surface.

Given the energy requirement for substrate transporters, as well as the expense of producing the membrane proteins themselves, it is desirable to know the total costs involved in import, as this must influence the success/failure of specific organisms in different environments. Although the requisite information for making such calculations appears to be lacking, it is clear what needs to be done. Knowing the number of atoms of a particular element comprising a newborn cell and the cell-division time, the total rate of cellular import can be computed, and if one is

willing to assume an energetic cost per imported molecule (e.g., two ATP hydrolyses per molecule), the total cost of the import process can be computed. If one knows the rate of transport per channel, one can also estimate the number of channels necessary for such transport, and given a knowledge of the proteins involved, the cost of synthesizing the transporters themselves can be estimated.

Using this approach, Phillips and Milo (2009) estimated that at saturating glucose concentrations (with an assumed transport rate of 100 glucose molecules / transporter / sec), $\sim 4\%$ of the membrane areas of *E. coli* cells must be allocated to glucose transporters. Assuming a 40 minute lifespan, and $\sim 2 \times 10^9$ glucose molecules to build a new cell, this implies: 1) a total cellular uptake rate of $\sim 833,000$ glucose molecules/sec, which at a transport rate of 100 molecules/sec, suggests the presence of $\sim 8,000$ glucose transporters per cell; and 2) a cost of glucose uptake per cell division of $\sim 4 \times 10^9$ ATP hydrolyses (assuming a cost of two ATPs per imported glucose molecule), which is $\sim 15\%$ of the total cost of building an *E. coli* cell. These numbers further imply a cost of import per transporter of $500,000$ ATP hydrolyses per cell division, which greatly exceeds the cost of building the transporters, as even a 1000 residue protein costs $\sim 30,000$ ATP hydrolyses (Chapter 17). All of these calculations are extremely rough, but they will hopefully motivate the need for future observations on numbers of transporters per cell, transport rates, and energetic costs of transport per cargo molecule.

Physiological acclimation. Care should be taken in the interpretation of estimates of nutrient-uptake parameters, as these are often derived from cells in various states of physiological acclimation, and it is known that uptake affinities can be developmentally variable. For example, when cells are acclimated to different nutrient conditions, and then assayed over a full range of nutrient concentrations, k_S is typically lower for cells previously exposed to nutrient-depleted medium (Collos et al. 2005), i.e., substrate affinity increases as the acclimation concentration decreases. In principle, such acclimation might be accomplished by regulation of transporter abundance per unit surface area. However, in many species, such physiological responses are associated with a developmental shift between the use of high- and low-affinity transporters, with the former being up-regulated in low nutrient conditions (Eide 2012).

Empirical observations with *S. cerevisiae* led Levy et al. (2011) to suggest that dual-transporter systems enable cells to more effectively respond to shifts to low-nutrient conditions. The idea here is that low-affinity transporters activate a starvation response more readily than do high-affinity transporters, and in doing so enhance the expression of high-affinity transporter genes, thereby enabling the cell to endure a longer period of nutrient scarcity. What remains unclear, however, is why the same dynamical response could not be achieved with a single high-affinity transporter system by simply up-regulating the transporter concentration in response to decreasing nutrient abundance.

An alternative explanation that may solve this puzzle invokes a tradeoff between the maximum rate of nutrient uptake and k_S in different isoforms (Gudelj et al. 2007), such that with limited membrane space available for transporters, the one with the highest affinity at the current substrate concentration is utilized. Such a tradeoff might arise if transporters operate in a bidirectional manner (Figure 18.1).

At high nutrient concentrations, high-affinity transporters can be saturated on both sides of the cell membrane, causing nutrient efflux to compete with influx, whereas low affinity transporters experience asymmetry, facilitating the net rate of influx (Bosdriesz et al. 2018). The resultant model, which allows the transporter binding-site conformation to switch from one side of the membrane to the other, leads to a modification of the normal Michaelis-Menten uptake kinetics. In contrast to uptake always increasing with the external substrate concentration, bidirectional flow results in a situation where for any particular transporter k_S, there is a substrate concentration at which the uptake rate is maximized. With the optimum concentration increasing with decreasing affinity (Figure 18.1), the model then predicts that lower-affinity transporters have higher rates of influx at higher external nutrient concentrations simply because they experience less conflict with internal cell concentrations.

Because genomes typically only encode for a small number of transporters for particular substrates, often no more than two, some peculiar behavior can arise under this model. Due to the existence of an optimal k_S for peak influx at any external nutrient concentration, the model predicts that for two transporters with k_S flanking the peak, there will always be a nutrient concentration at which both have equivalent influx rates. Notably, Wykoff et al. (2007) suggest that dual-transporter systems can exhibit bistable states, wherein at particular nutrient concentrations, a polymorphic (but clonally uniform) population of cells can be maintained. Although these authors view this sort of scenario to be the result of natural selection favoring a strategy for anticipating different types of nutrient-level changes, such an outcome may be nothing more than a physical consequence of the nature of the system.

Advantages of motility. Average swimming speeds in bacteria range from 10 to 100 μm/sec, whereas those in eukaryotic microbes are more on the order of 100 to 1000 μm/sec (Figure 16.4). There are numerous contexts in which swimming might confer an advantage, including predator avoidance and mate acquisition. In predatory species, motility will also increase the encounter rate of prey (Foundations 18.2), and when integrated with chemosensory systems, motility allows for habitat selection (Chapter 22).

Here, we simply explore the extent to which swimming can increase the rate of uptake of passively diffusing molecules. Recall that small ions have typical diffusion coefficients in the range of $D = 700$ to 2000 μm^2/sec, with an average value of 1300 μm^2/sec (Figure 7.6). If swimming is to substantially increase the rate of nutrient uptake, the product of the velocity (v) and the average distance between particles ($\bar{\ell}$), which has units of μm^2/sec, needs to exceed the diffusion coefficient of the harvested particles. Purcell (1977) called the ratio $\bar{\ell}v/D$ the stirring number (see also Zehr et al. 2017).

Assuming a random distribution, the mean inter-particle distance is approximately $[3/(4\pi S)]^{1/3}$, which is equivalent to the radius of a conceptual sphere having a volume per particle equal to the inverse of the substrate concentration, $1/S$. For example, a concentration of 1 mM, roughly the situation for inorganic carbon in seawater (Table 7.1), contains $\sim 600,000$ particles/μm^3, which implies an average distance between particles of $\bar{\ell} = 0.007$ μm. To match the average rate of ionic diffusion noted above, such that $\bar{\ell}v = D$, the swimming velocity ($D/\bar{\ell}$) would then need to

be $v \simeq 186,000$ μm/sec, far beyond the normal range in unicellular species. Similar calculations for a concentration of 1 μM (two to thirty times lower than average N and P concentrations in the ocean) lead to a critical speed of $\sim 18,600$ μm/sec, and for 1 nM (similar to the concentrations of a number of trace metals) the critical speed is $\sim 1,860$ μm/sec. Because cells swimming in low Reynolds-number environments drag along most of their boundary layer as they move (Berg and Purcell 1977), these are lower-bound estimates of critical swimming speeds. In addition, no consideration has been given to the energetic cost of swimming.

The overall implication here is that swimming by microbes generally does not greatly magnify the rate of intake of randomly distributed inorganic nutrients. A more formal analysis in Foundations 18.2 suggests a $< 5\%$ enhancement in bacteria, but potentially an up to two-fold inflation in large eukaryotic cells. Large organic compounds such as proteins have diffusion coefficients roughly $10\times$ smaller than those of inorganic ions, which would reduce the critical swimming velocities ten-fold, so depending on the environmental concentrations there may be some significant increases in their encounter rate. Thus, although the largest, fastest swimming eukaryotic cells may experience significant gains in the uptake rate of nutrients by enhanced stirring alone (Short et al. 2006; Solari et al. 2007), motility likely plays a greater role in active searches for resource gradients when coupled with chemoreception (Chapter 22).

Photosynthesis

Whereas the acquisition of dissolved inorganic molecules is important to cells, only a fraction of organisms can survive on such resources alone. Almost all of the global ecosystem ultimately depends on the conversion of solar energy into chemical energy directly used in the biosynthesis of organic materials. Organisms capable of such transformations are called phototrophs, in contrast to heterotrophs, which acquire their reduced carbon compounds from the former, either via uptake as single molecules or by bulk ingestion (phagocytosis or herbivory). Five other carbon-fixation mechanisms, not requiring light, are exploited by various groups of anaerobic prokaryotes (Thauer 2007; Berg et al. 2010; Fuchs 2011), and collectively all of these non-heterotrophs are called autotrophs. Approximately 99% of total global primary production is generated by RuBisCO, the key carbon-fixation enzyme in phototrophs (Raven 2009).

Photosynthesis is known to occur in seven bacterial phyla, but only in the cyanobacteria and photosynthetic eukaryotes does it result in oxygen release. In these cases of oxygenic photosynthesis, water is used as an electron donor in ATP recharging. The remaining groups of phototrophic prokaryotes are anoxygenic, relying on reduced inorganic compounds such as ferrous iron, hydrogen, and sulfur as electron suppliers, which in today's highly oxidized world are only locally abundant in a small number of environments. However, the atmosphere of the early Earth was anoxic and had CO_2 concentrations $100\times$ higher than in today's atmosphere, leading to the suggestion that anoxygenic photosynthesis was the first established form of phototrophy (Raven et al. 2017). Indeed, given its phylogenetic distribution

across bacteria, it may even have been present in the ancestral bacterium (Woese et al. 1985; Woese 1987), with many bacterial lineages subsequently experiencing loss and transition to heterotrophic life styles.

The origin of oxygenic photosynthesis was a key moment in evolutionary history, providing a means for exploiting a permanent and reliable supply of light energy to extract electrons from highly plentiful water molecules, using these to produce the ATP and NADPH necessary for the downstream synthesis of organic matter, and releasing O_2 in the process. The emergence and phylogenetic spread of oxygenic photosynthesis had a profound effect on the Earth's biogeochemistry, ultimately leading to a 10^5-fold rise of atmospheric O_2 concentration and a smaller, but still substantial, reduction of CO_2 levels (Figure 18.2). The first big phase of oxygenation, occurring ~ 2.5 billion years ago and presumably the result of the origin of photosynthetic cyanobacteria, dramatically raised the atmospheric O_2 concentration, albeit to a level $\simeq 5\%$ of today's atmosphere. It is thought that this set the stage for the evolution of oxygenic metabolism by aerobic heterotrophs (Lyons et al. 2014).

This new atmospheric state then remained relatively constant until ~ 750 million years ago, at which point there was a further elevation of O_2 concentration to today's level. This second quantum shift in atmospheric O_2 content was presumably a consequence of the origin of diverse groups of photosynthetic eukaryotes (including chlorophytes, red algae, diatoms, dinoflagellates, euglenoids, and haptophytes). All of these lineages acquired their photosynthetic capacities (embodied in chloroplasts) via horizontal transfers of endosymbionts ultimately of cyanobacterial origin (Shih 2015; Fischer et al. 2016; Chapter 23). During this second transition, there was a gradual draw-down of atmospheric CO_2 to today's level (which, despite the current uptick, is far lower than that 1 billion years ago).

The transformation of solar to chemical energy. As almost all of today's photosynthesis is carried out by aerobes, the remaining focus will be on oxygenic photosynthesis. The details of this complex system are outlined in most biochemistry texts, and only a gross overview will be provided. A key point is that the transition to oxygenic photosynthesis involved the emergence of two major innovations: the water-oxidizing photosystem II, which releases electrons, protons, and oxygen; and photosystem I, which utilizes the electron/proton output from photosystem II to drive the production of the energy carrying compounds ATP and NADPH. (The numbering system here is a historical artifact of the timing of discoveries).

Both photosystems are thought to date to a duplication event deep in the bacterial phylogeny, although the sequence similarity of their molecular constituents is so low as to raise considerable uncertainty on this interpretation. An additional issue is that the two photosystems coexist only in cyanobacteria and in the derived plastids of photosynthetic eukaryotes, although each individual system resides alone in a few other non-cyanobacterial groups. Thus, a key question is whether photosynthetic cyanobacteria uniquely joined the two systems via a horizontal transfer, or whether the dual system is ancestral, with other lineages containing just one having experienced loss of the other. Because all lineages of oxygenic photosynthetic bacteria appear to be derived within their phylogenetic groups, with no evidence for ancestral phototrophism within any group (even cyanobacteria) (Fischer et al. 2016; Shih

et al. 2017), the most parsimonious explanation is that multiple horizontal-transfer events occurred deep in bacterial phylogeny, one of which led to the dual I/II system in cyanobacteria.

Both photosystems are comprised of complexes of ~ 20 protein subunits and cofactors, which jointly carry out processes of light-harvesting, photoprotection, and transfer of electrons and protons. Two of the major photosystem-II proteins evolved by gene duplication prior to the diversification of the cyanobacteria and operate as heterodimers, whereas all bacterial photosystem-I complexes operate as homodimers, except in cyanobacteria where they are heterodimeric (Cardona 2015; Cardona et al. 2015).

The overall process of photosynthesis is further subdivided into the light reactions (carried out by the photosystems just noted) and the downstream carbon-fixation dark reactions (somewhat of a misnomer, as they can occur in light and dark). The quantum efficiency of the light reaction of photosynthesis, defined to be the number of moles of photons absorbed per mole of oxygen produced, is sometimes viewed as a universal constant. However, there is continuing disagreement as to its actual value (Melis 2009; Hill and Govindjee 2014), and although most estimates are in the range of 8 to 10 photons per O_2, it remains possible that this number differs among phylogenetic lineages. Taking the average, ~ 9 photons are required to convert two H_2O and two $NADP^+$ into one O_2, two protons, and two NADPH. The protons generated by this reaction are used to drive the production of ATP from ADP using a membrane-embedded ATP synthase (in essentially the same way that the analogous machine operates on the plasma membrane of bacteria and the inner mitochondrial membranes of eukaryotes; Chapters 2 and 17).

The carbon-fixation (dark) reactions, also known as the Calvin-Benson cycle, consume three molecules of CO_2 to produce one triose phosphate molecule (glyceraldehyde-3-phosphate) that can then be used in the synthesis of higher-order organic compounds. The process is a cycle in that a molecule of ribulose-1,5-bisphosphate (RuBP) is initially consumed, broken down, and then regenerated, yielding a net release of one glyceraldehyde-3-phosphate. This is an energy intensive process, with the production of each new triose phosphate requiring the investment of 6 NADPHs and 9 ATPs provided by the light reaction. This means that for the production of the 6 NADPHs needed to generate each triose phosphate, ~ 27 photons (4.5 for each NADPH, from the preceding paragraph) are required. If we assume that ~ 3 protons are required for the production of each ATP (Chapters 2 and 17), then 27 protons and ~ 122 photons (4.5 per proton, from above) are required per triose phosphate. Thus, in total, $\sim 27+122 = 149$ photons are required for the production of each triose phosphate, i.e., ~ 50 photons per fixed carbon atom.

Not all wavelengths of light are utilized by photosynthetic organisms. Using chlorophylls a and b, along with a set of accessory pigments, all arranged within a reaction center in the large photosystem complexes, most photosynthesis relies on photons from the 400 to 700 nm wavelength range of the solar spectrum (essentially the visible spectrum). However, not all wavelengths of light are utilized with equal efficiency, and substantial energy in the infrared range of sunlight goes unharvested by most plants. A few photosynthesizers such as the cyanobacterium *Acaryochloris* have an accessory pigment that expands the range of availability up to 750 nm (Chen and Blankenship 2011), but it remains unclear why the vast majority of

photosynthesizers leave this resource untouched.

The world's most abundant enzyme. The centerpiece of the Calvin-Benson cycle in photosynthesis is RuBisCO (ribulose-1,5-bisphosphate carboxylase / oxygenase), the enzyme that catalyzes the joining of ribulose-1,5-bisphosphate (RuBP, a five-carbon molecule) and CO_2 into the six-carbon product that is subsequently split into two three-carbon molecules (glyceraldehyde-3-phosphates). The latter are then deployed in downstream biosynthetic pathways as well as in the recycling of RuBP for another round of carbon fixation. As the major generator of primary organic material in the biosphere, RuBisCO is thought to be the most abundant protein on Earth, summing to $\sim 0.7 \times 10^{12}$ kg, 95% of which is in terrestrial plants (Bar-On and Milo 2019).

Given the enzyme's conserved role across biology, RuBisCO exhibits a surprising level of structural diversity. Phylogenetically, the enzyme consists of two major variants. Form I (a hexadecamer, consisting of a ring of eight large subunits, capped off on both ends by rings of four small subunits) is found in most eukaryotic algae and cyanobacteria. Form II (no small subunits) is found in anaerobic photosynthetic proteobacteria and dinoflagellates, each of which has multiple structural variants (Morse et al. 1995; Erb and Zarzycki 2018). Moreover, there are additional variants in prokaryotes. In the photosynthetic bacterium *Rhodopseudomonas palustris,* RuBisCO is a homohexamer, whereas in *Rhodospirillum rubrum,* it is a homodimer. In the two Archaea in which a form of RuBisCO is known, in one case it is an homooctamer (*Pyrococcus horikoshii*), and in another case it is a homodecamer (*Thermococcus kodakaraensis*) (Maeda et al. 2002). The evolutionary roots of RuBisCO remain unclear, but the presence of RuBisCO-like proteins with other functions in various bacterial and archaeal lineages suggests that CO_2-fixing RuBisCO may be derived from a protein with quite different features, possibly nucleotide assimilation (Ashida et al. 2005; Erb and Zarzycki 2018).

Despite the energetic expense of photosynthesis, RuBisCO is a surprisingly inefficient enzyme. As there are many applied reasons for understanding the mechanisms of photosynthesis, e.g., in agriculture, the uptake kinetics of RuBisCO have been studied in a broader phylogenetic context than any other enzyme, usually by evaluating *in vitro* performances of isolated complexes. Estimates of k_{cat} (a measure of the maximum processing rate per enzyme molecule; Chapter 19) for CO_2 range from 1 to 5/sec in photosynthetic eukaryotes, with those in prokaryotes ranging from 5 to 14/sec (Uemura et al. 1997; Tcherkez et al. 2006; Savir et al. 2010; Galmés et al. 2014a,b), orders of magnitude below the possible values based on biophysical limitations. Likewise, $k_{\text{cat}}/k_{\text{S}}$ (a measure of efficiency of processing at non-saturating conditions) for CO_2 ranges from 10^5 to 5×10^5 $\text{mol}^{-1}\text{sec}^{-1}$ in eukaryotes, and from 10^4 to 2×10^5 $\text{mol}^{-1}\text{sec}^{-1}$ in bacteria, in both cases far below the diffusion limit expected for a perfect enzyme (Chapter 19). These low turnover rates per catalytic site necessitate that RuBisCO be maintained at high intracellular concentrations, further magnifying the cost of relying on this large enzyme. Moreover, the *in vitro* measures belie the actual situation in nature. Relative to maximum-capacity measurements of RuBisCO in the laboratory, the global time-average performance of the enzyme in nature is just 1% for terrestrial and 15% for marine environments (Bar-On and Milo 2019).

A large part of the problem here is that RuBisCO is a remarkably error-prone enzyme. As implied by its designation as a carboxylase/oxygenase, the enzyme competitively binds both CO_2 and O_2, with the latter event resulting in the production of a toxic by-product that is eliminated by a process called photorespiration. Assuming that substrate molecule concentrations are less than saturating, the error rate of RuBisCO resulting from encounters with oxygen molecules is a function of the specificity ratio, which is equivalent to the ratio of the uptake affinities, $k_{\rm cat}/k_{\rm S}$, for the two substrates,

$$R_{O_2/CO_2} = \frac{k_{\rm cat,O_2}/k_{\rm S,O_2}}{k_{\rm cat,CO_2}/k_{\rm S,CO_2}}. \tag{18.2a}$$

Estimates of R_{O_2/CO_2} for RuBisCO from eukaryotes fall in the range of 0.005 to 0.015, whereas those for prokaryotes range from 0.02 to 0.10. Thus, if confronted with equal concentrations of the two gases, the error rate would be in the range of a few percent. Whereas this may not seem like an overly large problem, the total error rate is a function of the product of the specificity ratio and the ratio of substrate concentrations, C_{O_2/CO_2},

$$E_{O_2/CO_2} = \frac{R_{O_2/CO_2} \cdot C_{O_2/CO_2}}{1 + (R_{O_2/CO_2} \cdot C_{O_2/CO_2})} \simeq R_{O_2/CO_2} \cdot C_{O_2/CO_2}, \tag{18.2b}$$

where the final approximation applies if $R_{O_2/CO_2} \cdot C_{O_2/CO_2} \ll 1$. Today's atmosphere imposes much higher concentrations of O_2 than CO_2, ~ 250 and 7 μM in saturated water respectively, so $C_{O_2/CO_2} \simeq 36$. This implies astoundingly high error rates, e.g., in the range of 0.15 to 0.35 for eukaryotes. As discussed below, cellular mechanisms for concentrating CO_2 intracellularly have evolved to mitigate this problem, but such embellishments impose additional layers of cellular investment.

The underlying factors responsible for these suboptimal features of RuBisCO remain unclear. Phylogenetic reconstructions of ancestral states and evaluation of their biochemical features suggest that the addition of the small capping subunits to produce Form I enzymes led to both increased affinity and specificity for CO_2 prior to the great oxygenation event (Schulz et al. 2022). However, whereas such results suggest that Form I RuBisCOs may have been preadapted to changing atmospheric conditions, the enduring oxygen sensitivity of the enzyme for the past two billion years is left unexplained.

Tortell (2000) suggested an adaptive basis for an observed gradient between R_{O_2/CO_2} and the estimated geological age of a phylogenetic group, with a decrease from ~ 0.02 in ancient cyanobacterial lineages to 0.005 in the more recent diatom lineage (although red algae are a clear outlier). They argue that the enzyme evolved higher CO_2 specificity in more recent lineages as atmospheric CO_2/O_2 ratios declined (Figure 18.2). However, the assumption here is that RuBisCO initially evolved in bacteria inhabiting anoxic environments, and then remained frozen in the ancestral form in descendent cyanobacteria, whereas it became free to evolve in new directions in eukaryotic lineages following the great oxidation event (~ 2.5 billion years ago). Recalling the points made above for nutrient uptake, i.e., the well-known ability of microbes to evolve metabolically on time scales of thousands of generations, the likelihood of enzymatic features remaining frozen with suboptimal features for millenia is very small. Moreover, the frozen-accident hypothesis is inconsistent with broad phylogenetic analyses suggesting substantial adaptive amino-acid substitutions in

RuBisCO, including on the dimeric interfaces near the active sites of the enzyme (Kapralov and Filatov 2007; Young et al. 2012; Poudel et al. 2020).

A common, alternative narrative is that the low efficiency and error-prone nature of RuBisCO is an inevitable consequence of structural constraints. Under this view, the enzyme actually has near optimal performance conditional on the unavoidable compromises. Most notably, a suggested negative correlation between the catalytic affinity for CO_2 and the ability of the enzyme to discriminate against O_2 motivates the view that simultaneous improvement in both features is structurally difficult (Tcherkez et al. 2006; Savir et al. 2010; Shih et al. 2016; Flamholz et al. 2019). Catalytic affinities and specificities for CO_2 vary by more than an order of magnitude across species, but do so in a phylogenetically dependent manner. Cyanobacteria are at one extreme, having high maximum rates of carboxylation but low specificities for CO_2, whereas the red algae are at the opposite end of the spectrum, with chlorophytes having intermediate values of both. However, it has been argued that confidence in the constraint argument has been inflated by a failure to account for the phylogenetic structure in the data, with the statistical correlations between RuBisCO kinetic parameters being largely due to differences between (rather than within) eukaryotic and prokaryotic groups (Bouvier et al. 2021). In addition, the proposed mechanistic constraint has not yet been demonstrated empirically.

As alluded to above, there is an additional determinant of CO_2-utilization efficiency by RuBisCO – the ratio of O_2 to CO_2 concentrations of the two substrates at the active site of the enzyme, C_{O_2/CO_2}. Many species reduce the latter via a CO_2-concentrating mechanism (CCM) for increasing the internal availability of CO_2 (Beardall and Giordano 2002; Falkowski and Raven 2007). Such mechanisms are best known in land plants harboring C_4 and CAM (crassulacean acid) metabolisms. In the latter cases, CO_2 is incorporated into malate in spatially or temporally separate contexts from RuBisCO, which subsequently receives its CO_2 payload after malate dissociation. Malate formation appears to have been evolutionarily modified into a CCM many dozens of times independently in land plants (Brown et al. 2011; Heyduk et al. 2019), as well as in various unicellular lineages (Raven et al. 2017). For example, cyanobacteria concentrate CO_2 locally into microcompartments housing the photosynthetic apparatus (carboxysomes).

Because an efficient CCM will offset a higher intrinsic error rate, RuBisCO evolution provides another potential example of a bivariate drift barrier. Indeed, there is a strong inverse relationship between the specificity factor and CCM factor across species (Badger et al. 1998), i.e., species with a strong capacity to concentrate CO_2 have less discriminating RuBisCOs. In addition, species with high specificity factors produce less RuBisCO (Hobson and Guest 1983). Thus, the overall patterns are consistent with the evolutionary-layering hypothesis (Lynch and Hagner 2014), which postulates that an increase in complexity need not ultimately yield an increase in overall system performance, as the addition of a layer in a molecular pathway alleviates the intensity of selection operating on prior components.

If nothing else, these observations on one of the biosphere's most important proteins provide some cautionary notes for those who fully subscribe to the adaptive paradigm that all biological features have been molded to absolute perfection by the relentless pressure of natural selection. Are certain regions of phenotypic space empty (e.g., high CO_2 affinity and specificity in the case of RuBisCO) because

such phenotypes are absolutely unattainable on biophysical grounds, or because once produced the selective advantages are so weak or the mutational biases in the opposite direction so strong that they cannot be maintained in natural populations?

Biotechnology industries are built on the assumption that nature can be improved upon. With respect to engineering more efficient RuBisCO molecules with greater catalytic efficiency and speed, some improvements have been made with as few as one or two amino-acid substitutions, although these have not yet translated into increased productivity of recipient (crop) species (Spreitzer and Salvucci 2002; Greene et al. 2007; Gomez-Fernandez et al. 2018; Wilson et al. 2018; Zhou and Whitney 2019). Whereas such progress may seem unimpressive, it should be kept in mind that the period of investigation extends over just a 20-year period, in contrast to > 2 billion years of evolution of RuBisCO in nature. Notably, the existence of less than perfect enzymes is not restricted to RuBisCO, and there are success stories with respect the laboratory improvement of enzyme performances, e.g., a substantial increase in the efficiency of superoxide dismutase (Stroppolo et al. 2001), as will be discussed further in the following chapter.

Osmoregulation

Although cells often experience dramatically different environments on within- and between-generation time scales, they often go to extremes to ensure that internal physiological operating conditions remain relatively constant. Because the structure and function of proteins depends on their surrounding chemistry, to operate in an efficient manner, cells must regulate the concentrations of their constituents, including hydrogen ions and all other dissolved substances. Among other things, this raises the necessity of osmoregulation. Hyperosmotic (saline) environments promote cell dehydration, excess molecular crowding, and reduced levels of molecular diffusion. In contrast, hypoosmotic environments induce cell swelling and potential membrane rupture.

Water can pass through cell membranes at potentially very rapid rates, owing to the presence of membrane-spanning pores called aquaporins, which passively admit water molecules while excluding other ions. Because aquaporins are present across the entire Tree of Life, with the apparent exception of some thermophilic bacteria (Abascal et al. 2014), they were likely present in LUCA. In eukaryotes, they have diversified into two major groups, one of which engages in glycerol transport for reasons discussed below. However, osmoregulation is not a simple matter of regulating the number aquaporin channels. Much of it involves the active transport and/or production of solutes.

For bacterial cells completely surrounded by a cell wall, the natural tendency for cell-volume expansion by water entry is countered by wall resistance. However, the resultant equilibrium turgor pressure by no means eliminates problems with osmotic stress, particularly when the environment is hyperosmotic. Because there are no active pumps for water molecules in bacteria, osmoregulation requires continual environmental sensing and, when necessary, rapid fluxes of ions and/or the production of osmolytes (Bremer and Krämer 2019). Commonly synthesized solutes

are small organic compounds such as glycerol, proline, glycine betaine, and sucrose, which have no effects on the performance of active molecules and hence are called compatible solutes (Figure 18.3). Such molecules can also be expelled rapidly if the external medium is too hypoosmotic.

The power of cell walls for reducing the costs of osmotic balance is illustrated by a class of phenotypic variants in numerous bacterial species called L-form cells (Errington et al. 2016; Errington 2017; Claessen and Errington 2019). Such wall-less cells are induced by chronic exposure to antibiotics that interfere with peptidoglycan production. However, the maintenance of L-form cultures requires an osmoprotective medium (usually achieved by the addition of sucrose, which is not metabolized). Given that many eukaryotic lineages have abandoned cell walls, long-term evolution experiments to gradually wean L-forms from dependence on a hyperosmotic environment would help reveal how secondary accommodations emerge to affect such a radical change in cellular structure. Given the high energetic costs of cell walls (Chapters 16 and 17), the development of stable cultures of such cells may also have utility in biotechnological applications.

Oren (1999) calculated the costs of osmoregulation in halophilic bacteria using compatible solutes vs. ionic balance. The compatible-solute strategy requires the intracellular synthesis of organic osmolytes, whereas the ion-balance strategy requires the flux of appropriate ions across the plasma membrane. Mixtures of the two strategies occur, and such regulation is especially important in marine and other hypersaline environments. Depending on the costs of alternative strategies, different species may be favored in some environments and excluded from others.

The biosynthetic costs per compatible-solute molecule (in units of ATP hydrolyses) range from 20 to 66, increasing with increasing molecular weight of the compound (Figure 18.3). Based on the molarity of compatible solutes in cells of marine microbes, this led Oren (1999) to suggest that up to 85% of the construction cost of a halophilic cell may be associated with osmoprotection. Given these substantial investments for organisms inhabiting saline environments, it remains unclear why variation among organisms exists for the compatible solutes deployed. Glycerol is the cheapest solute to produce, and also has the highest solubility. However, although relied upon by yeast and the marine alga *Dunaliella,* which has specialized membranes, glycerol is a challenge because of its ability to permeate most membranes. Many nonhalophilic bacteria utilize sucrose or trehalose.

Equally unclear is why most species rely on compatible solutes at all (as opposed to maintaining ionic balance). Although the data are scant, as noted above, most specialized transporters appear to require one to two ATP hydrolyses for the forward movement of each transported molecule (Oren 1999; Patzlaff et al. 2003; Lycklama A Nijeholt 2018). Species that regulate osmotic pressure with ion balance often do so by modulating the cellular concentration of KCl. Potassium and chloride ions are imported through specific transporters, coupled with sodium export and proton input. The cost of import appears to be on the order of 0.5 to 0.67 ATP hydrolyses per KCl imported, 35 to 160× lower than the cost of synthesizing a compatible-solute molecule. These calculations do not include the costs of the machinery necessary to carry out these processes, which might be greater in total for Na^+/H^+ antiporters and K uniporters than for the biosynthetic machinery for compatible solutes.

Wall-less cells (most eukaryotes) face additional problems with osmotic pressure.

To retain high levels of intracellular solutes, there is a need for a mechanism for removal of water molecules that work themselves through the membrane. This problem is magnified greatly in cells engaging in phagocytosis and the inevitable consumption of the external medium. Among flagellated eukaryotes, even walled cells have a water problem, as the flagella are surrounded by lipid bilayers (but not by walls) providing an entry for water molecules. Many eukaryotes deal with this relentless import of water by use of a contractile vacuole, which grows in volume by accumulating excess cell water, and then periodically ejects its contents into the surrounding medium. How this is accomplished in a way that selectively retains key cytoplasmic constituents remains unclear, although a number of hypotheses have been suggested (Raven and Doblin 2014).

The amount of water expelled by eukaryotic cells is impressive. For example, Lynn (1982) found a positive scaling of the volume of the contractile vacuole and cell volume in ciliates, with the total rate of volumetric output (μm^3/day) scaling as $460V^{0.88}$, where V is the cell volume (in μm^3). For the range of ciliate cell sizes studied, $\sim 10^4$ to 10^6 μm^3, this relationship implies that between 152 and 87 cell volumes of water are ingested (and expelled) per day. Even higher rates have been found in other organisms. For the green alga *Chlamydomonas reinhardtii,* with a cell volume of $\sim 140\,\mu m^3$ and an average expulsion rate of 38,000 μm^3/day (Raven 1982; Buchmann and Becker 2009), the implied number of cell volumes ingested (and expelled) per day is 270. Another green alga *Mesostigma viride,* which harbors eight contractile vacuoles, expels 1150 equivalents of its volume per day (Buchmann and Becker 2009).

A deeper understanding of the magnitude of these demands can be obtained from expressions for the flow rate of water across a membrane of known porosity separating two liquids with different osmolarities (Foundations 18.3). Such analyses lead to the conclusion that a very substantial fraction of eukaryotic cell-maintenance requirements must be devoted to osmoregulation. The overall implication here is that, owing to different osmotic demands and the evolved mechanisms for dealing with them,environments with different salinities will substantially alter the growth performance of organisms even in the face of equivalent levels of critical resources.

Circadian Rhythms

Most multicellular organisms use internal molecular clocks to generate circadian rhythms. In effect, such time keepers enable organisms to predict the short-term future and make gene-expression and physiological changes appropriate to the demands of day/night (light/dark) cycles. The definition of a circadian system is somewhat subjective, but the central feature is some form of robust rhythmicity, with a near 24-hour periodicity that can be accurately entrained by an external factor (such as a light:dark cycle) but can also remain free-running for extended periods in a constant environment. A lack of the periodicity's sensitivity to absolute temperature (unlike most biochemical properties) is generally taken to be a hallmark of a true circadian rhythm.

Most multicellular organisms have generation lengths of weeks to years, so such

diurnal cycles occur many times throughout the life of the individual. However, in unicellular species, minimum cell-division times can be much less than 24 hours. In this case, individual cells commonly complete their entire lives in very different periods of the diurnal cycle, raising questions as to the utility of a molecular clock in such species. Nevertheless, they do exist.

Circadian rhythms are known to exist in numerous unicellular phototrophs including green and red algae, dinoflagellates, and euglenoids (Roenneberg and Merrow 2001; Brunner and Merrow 2008; Noordally and Millar 2015). Eelderink-Chen et al. (2010) found that imposition of a temperature cycle can entrain a circadian rhythm in the yeast *S. cerevisiae,* although the cycle is damped within just two days of constant temperature. A day:night circadian rhythm is also loosely coupled to the mitotic cell cycle in the filamentous fungus *Neurospora,* albeit with cell division being far from synchronous (Hong et al. 2014). Although few of the details have been worked out, the time-keeping mechanism in all of these cases is thought to involve rhythmicity in clock-component gene transcription, as is known in land plants and metazoans. In multiple eukaryotes (humans, green algae, and filamentous fungi), rhythmicity appears to be governed by intracellular levels of magnesium, which operates as a cofactor with ATP and can therefore globally influence cellular features such as translation rates (Feeney et al. 2016).

Although the existence of entrainable clocks in heterotrophic bacteria is circumstantial at best (Sartor et al. 2019), the cyanobacterium *Synechococcus* has a well-characterized circadian clock, with a simple mechanism quite unlike that in eukaryotes (Figure 18.4). Indeed, the core oscillator can be made to operate *in vitro* in a solution containing just three proteins (KaiA, KaiB, and KaiC) and ATP (Nakajima et al. 2005; Phong et al. 2013), which engage in a cycle of post-translational modifications. The central hub, KaiC, is phosphorylated in the presence of KaiA, but once this occurs, KaiB forms a complex with KaiC that inhibits KaiA, thereby promoting dephosphorylation of KaiC, starting the cycle anew. This cycle further elicits a signal-transduction cascade (Chapter 22) of gene-expression events leading to growth-inhibition in the absence of light. Also of note is that KaiC is a homohexamer. Although the phosphorylation of individual KaiC molecules is a stochastic process, the hexamers dissociate and reassociate, leading to homogenization of their phosphorylation states and hence a more coherent signal (Kageyama et al. 2006).

The protein-driven *Synechococcus* clock is different from that typically observed in eukaryotic systems, which are generally based on negative feedback resulting from activation of genes whose products ultimately repress their own expression. The cycle seems to be set by metabolic oscillations determined by diurnal resource availability, and hence is only indirectly correlated with the light:dark cycle itself (Pattanayak et al. 2015). As with the clocks of land plant and animals, however, the *Synechococcus* circadian rhythm can track changes in the day:night cycle even in an *in vitro* setting, providing a built-in response to seasonal changes (Leypunskiy et al. 2017). On the other hand, exposure to short pulses of darkness reset the clock in inappropriate ways, decreasing cell division rates (Lambert et al. 2016), raising a second issue.

A key challenge for circadian clocks is the sensitivity to internal and external noise. The former derives from small numbers of molecules per cell and bursty transcription, while the latter results from weather effects such as cloud coverage.

Internal noise is expected to be more significant for species with smaller cells, which naturally harbor smaller numbers of proteins. Thus, it is of interest that *Prochlorococcus,* a marine cyanobacterium that is significantly smaller than *Synechococcus,* does not have a free-running circadian clock. Instead, *Prochlorococcus* deploys an hourglass-like clock, which responds directly to each daily change in light:dark and does not run freely in the absence of a daily signal. This shift is a consequence of the absence of the negative-feedback component KaiA in *Prochlorococcus* (Holtzendorff et al. 2008).

There is indirect evidence that this kind of shift in clock structure may be adaptive in small-celled species. When the internal noise is sufficiently large, free-running clocks are perturbed enough by noise amplification in the negative-feedback loop to become more unreliable than hourglass clocks that are naturally reset each day. On the other hand, free-running clocks appear to be less vulnerable to large-amplitude fluctuations in external signals (Chew et al. 2018; Pittayakanchit et al. 2018). The effects here are not large, however, and it remains to be shown whether the stochasticity of the clocks in these alternative systems have adaptive consequences.

How much does it cost to run and maintain a molecular clock? Although the details remain to be worked out, progress can be made in the example given above, as it appears that the vast majority of the cost is associated with the biosynthesis of the proteins involved. The Kai system is driven by ATP hydrolysis, but the 24-hour cycle involves the hydrolysis of just 60 ATP molecules per hexamer (Terauchi et al. 2007). Because each monomer of the KaiC hexamer consists of 518 amino acids, with a biosynthetic cost of ~ 30 ATP hydrolyses per amino acid (Chapter 17), provided the cell-division time is a day or less, it is clear that the biosynthesis of the Kai components constitutes almost all of the cost.

Chew et al. (2018) estimate there to be $\sim 4,000$ KaiA molecules/cell (284 amino acids each), $11,000$ for KaiB (102 amino acids), and $8,000$ for KaiC. Assuming a total cost of ~ 30 ATPs per amino acid, implies a total biosynthetic cost $\simeq 2 \times 10^8$, as compared to the $\sim 5 \times 10^5$ for running the clock. Using Equation 8.2b, the cost of building a *Synechococcus* cell (with volume $\sim 0.5\ \mu\text{m}^3$) is $\sim 14 \times 10^9$ ATP hydrolyses, so on the order of 1.5% of the construction energy budget is consumed by building and running the clock.

A similar computation can be made for the diminutive marine green alga *Ostreococcus,* which has a cell volume $\simeq 1.7\ \mu\text{m}^3$, and therefore requires $\sim 45 \times 10^9$ ATP hydrolyses to build a cell. The clock in this species runs by a simple transcriptional-loop mechanism, with one protein (CCA1) repressing the transcription of another (TOC1), and the latter activating transcription of the former (Bouget et al. 2014). The circadian cycle is driven by protein degradation, with the number of CCA1 protein copies cycling from 100 to 400 per day, and of TOC1 proteins cycling from 10 to 150 per cell (van Ooijen et al. 2011). Thus, the protein degradation rates are 0.75 and 0.93, respectively. Letting the proteins be ~ 300 and 500 in length, and assuming one cell division per day, using Equation 17.4, which assumes amino acids are recycled, leads to estimates of total costs of protein production of 3.6×10^6 and 2.2×10^6 ATP hydrolyses for CCA1 and TOC1. Together, these constitute just 0.01% of the cell's total energy budget. A number of costs are ignored here, but their inclusion would be unlikely to increase this estimate by more than an order of magnitude. For example, although the cost of transcription has been ignored, this is

known to be on the order of 10% of the protein-level cost (Chapter 17). The clock in this species seems to run via non-transcriptional rhythms of a light-sensitive protein (O'Neill et al. 2011), which could further increase the cost several fold. However, the central point seems to remain – the overall cost of running a clock in this species is kept very small because of the low number of proteins involved. Recall, however, that were there to be an advantage of losing a clock, a bioenergetic advantage of 1% would be quite easily promoted by natural selection.

Finally, it is worth emphasizing the elegant simplicity of the few molecular clocks that have been dissected in microbial species, in contrast to the extraordinarily baroque multi-loop constructs deployed by animals. Not only are the pathways more complex, elongated, and mechanistically diverse, but metazoans appear to have multiple clocks for different subcellular features (Mofatteh et al. (2021). Combined with the basic Cdk/kinase oscillator deployed in the cell cycle (Chapter 10), the latter can be intertwined, often with one master clock locking in the phasing of others. Some subsidiary clocks have cycle lengths that are harmonics of the usual 24-hour periodicity, e.g., 8- or 12-hour periods, and some can be made to run autonomously with respect to others.

There is no evidence that the embellishments of complex clocks in multicellular species are more efficient, and they are certainly more energetically costly. This lead one author to dub them an example of a "Rube Goldberg" construct (Sancar 2008), after the cartoonist famous for his creation of extraordinarily complex machines to carry out simple tasks. As has been seen in prior chapters and will continue to emerge in those following, this seemingly gratuitous increase in the complexity of molecular mechanisms is a hallmark of multicellular organisms. Rather than being driven by adaptive processes, it has likely accrued in a nonadaptive manner as a passive consequence of the change in the population-genetic environment of such lineages. The emergent traits remain critical to organismal well-being, but gradually accrue aspects of overdesign.

Summary

- Of the ~ 20 chemical elements essential for growth, almost all are enriched intracellularly relative to environmental levels. It has been suggested that low environmental concentrations of elements can encourage selection for genome-wide enrichment of particular nucleotides depauperate for such elements. However, the selection differentials at the single-nucleotide level are so small that this is unlikely to occur in even the largest prokaryotic populations. On the other hand, selection for/against usage of particular amino acids with extreme elemental compositions is feasible in some unicellular species with very large effective populations sizes.

- Nutrient-uptake affinities increase with cell volume across species on a per-cell basis, but decline on a per-biomass basis. Although the data are limited, $> 10\%$ of cell energy budgets is allocated to the physical process of nutrient uptake,

and many species acclimate to their surrounding nutrient levels by deploying membrane-bound transporters with different levels of substrate affinity.

- In large eukaryotic cells, swimming can increase rates of nutrient uptake by overcoming diffusion limitations. However, the effects are small in bacterial sized cells, suggesting that the primary function of motility involves other factors such as the movement up resource gradients by chemotaxis.

- The process of oxygenic photosynthesis, responsible for the fixation of almost all of Earth's carbon, is an energetically expensive process. It is carried out by RuBisCO, probably the world's most abundant protein, but also one of the least efficient and most error-prone of all known enzymes. It remains unclear whether the latter features are consequences of biophysical constraints.

- To keep their internal conditions at near-optimal states for physiological function, all cells have a variety of homeostatic mechanisms. Osmoregulation is a perpetual problem for cells, as internal solute concentrations are generally unequal to those in the external environment. Cell walls counter the osmotic stress confronted by many species, but wall-less species (many eukaryotes) must continuously pump water out, often with a daily export equivalent to 100 to 1000 cell volumes. The relative costs of structural (wall) vs. dynamical (pump) solutions to the osmoregulation problem remain to be worked out, but both consume a considerable fraction of cellular resources.

- Despite having cell-division times that are typically < 1 day, a number of unicellular species have independently evolved internal clocks with 24-hour periodicities, which provide a basis for predicting and preparing for diurnal environmental changes. Although only understood in a few species, the molecular mechanisms appear to consume no more than 2% of a cell's daily energy budget, and most of this is associated with construction rather than running of the clock. The molecular details of clocks in unicellular species are striking in their simplicity relative to the baroque mechanisms deployed in multicellular species.

Foundations 18.1. The response of uptake rate to nutrient concentration. Because the uptake of a molecule is typically carried out by specific membrane-bound nutrient transporters, the total rate of uptake by a cell is expected to scale positively with both the number of transporters residing in the cell membrane and the nutrient concentration at the surface of the cell. The latter, however, is not the same as the concentration in the bulk medium. As nutrients at the cell surface are constantly being taken up, there is a natural concentration gradient away from the cell surface governed by the rate of nutrient diffusion. Thus, one way of achieving a mechanistic understanding of the cellular rate of nutrient uptake is to first consider the transporter-based uptake kinetics conditional on the nutrient concentration at the cell surface, and then to relate the latter to the external diffusion process (Armstrong 2008).

Letting f denote the fraction of transporters on the cell surface engaged with a substrate molecule, t_h be the handling time of a captured molecule (the time to transport the molecule to the cytoplasm), k_c be the capture rate of a substrate molecule by an unengaged transporter, and S_0 be the nutrient concentration at the cell surface, the rate of change in transporter occupancy is

$$\frac{df}{dt} = k_c S_0(1-f) - f/t_h. \tag{18.1.1a}$$

At steady state, $df/dt = 0$, and rearrangement of Equation 18.1.1a yields a mean fraction of occupied transporters

$$\widetilde{f} = \frac{S_0}{[1/(k_c t_h)] + S_0}, \tag{18.1.1b}$$

which asymptotically approaches 1.0 as $S_0 \to \infty$. With n_T transporters per cell surface, and each engaged transporter handling its cargo at rate $1/t_h$, the total rate of nutrient uptake is then

$$V = \frac{n_T \widetilde{f}}{t_h} = \frac{V_{\max} S_0}{k_T + S_0}, \tag{18.1.2}$$

with $V_{\max} = n_T/t_h$ being the maximum uptake rate (achieved when all transporters are engaged), and $k_T = [1/(k_c t_h)]$ being the nutrient concentration at the cell surface at which the uptake rate is half the maximum value.

Although Equation 18.1.2 has the convenient Michaelis-Menten form, as in Equation 18.1, the substrate concentration is inconveniently that at the cell surface, S_0. The next step is to determine the expected nutrient concentration at the cell surface, S_0, conditional on the measurable concentration in the bulk medium, S_∞. Pasciak and Gavis (1974) noted that at steady state, the transport-limited flux rate into the cell (noted above) must be equivalent to the delivery rate of the nutrient to the cell surface. The latter can be obtained by use of Fick's law (Foundations 7.2), which states that the flux rate of a diffusing substrate across a point is equal to the product of the concentration gradient at that point and the diffusion coefficient,

$$F = D \cdot (\partial S_d/\partial d)|_{d=r_e}, \tag{18.1.3a}$$

where D is the diffusion constant for the substrate, r_e is the effective radius of the cell (which can be obtained from the cell volume, assuming a sphere), and d is the distance from the center of the cell. To obtain the concentration gradient, we assume an asymptotic approach to the bulk fluid concentration (S_∞) with distance d, starting with the concentration at the cell surface, S_0,

$$S_d = S_0 + (S_\infty - S_0)\left(1 - \frac{r_e}{d}\right), \tag{18.1.3b}$$

which has the properties of $S_d = S_0$ when $d = r_e$, and $S_d \to S_0$ as $r_e/d \to 0$. The concentration gradient is then

$$\frac{\partial S_d}{\partial d} = \frac{r_e(S_\infty - S_0)}{d^2}. \tag{18.1.3c}$$

Substituting into Equation 18.1.3a, with $d = r_e$, the flux per unit surface area of the sphere is found to be

$$F = D(S_\infty - S_0)/r_e, \tag{18.1.3d}$$

and multiplication by the cell surface area $4\pi r_e^2$ yields

$$V = (4\pi r_e)D(S_\infty - S_0). \tag{18.1.3e}$$

This shows that the total flux rate to the cell is proportional to r_e, rather than the surface area of the cell, because of the inverse relationship between the flux rate per surface area and r_e.

Often Equation 18.1.3e is multiplied by a dimensionless Sherwood number (Sh), which accounts for effects on the diffusion rate resulting from the deviation of the actual cell shape from a sphere and from other active processes that magnify the movement of substrate molecules relative to the case of pure diffusion (e.g., swimming). In other words, Sh is defined as the ratio of the realized rate of uptake to the expectation under diffusion alone. Defining the Péclet number as $Pe = 2r_e v/D$, where $2r_e$ is the length of the cell, v is the swimming velocity, and D is the diffusion coefficient, $Sh \simeq [1 + (1 + 2Pe)^{1/3}]/2$ (Guasto et al. 2012).

Equation 18.1.3e assumes $Sh = 1$, and for the remaining formulae, we will suppress the use of Sh, noting that where desired it can simply be inserted as a prefactor for D. However, to gain some appreciation for the degree to which swimming can enhance nutrient uptake, recall from Figure 7.6 that $D \sim 10^3 \mu\text{m}^2/\text{sec}$ for small ions. From Figure 16.4 a typical swimming speed for a bacterial cell with volume 1 μm^3 (which implies $2r_e \simeq 1.2$ μm) is $v = 50\,\mu$m/sec. This implies a Péclet number of 0.06, and a Sherwood number equal to 1.02, i.e., a 2% increase in the rate of nutrient uptake. For a eukaryotic cell of volume 10^4 μm^3 ($2r_e \simeq 120$ μm) and velocity $300\,\mu$m/sec, the Péclet number becomes 36, yielding a Sherwood number of 2.6. Thus, by breaking down the diffusion barrier by swimming, large (phytoplankton-sized) cells are capable of a substantial increase in the rate of nutrient uptake. This, of course, needs to be tempered by the increased cost of swimming.

Finally, rearranging Equation 18.1.3e to solve for S_0 and substituting the latter into Equation 18.1.2 yields the expected uptake rate

$$V = \frac{V_{\max}(V - D'S_\infty)}{V + (k_T - S_\infty)D'}, \tag{18.1.4a}$$

where $D' = D(4\pi r_e)$. Although Equation 18.1.4a is a quadratic equation, making the solution for V somewhat complicated, Armstrong (2008) found that a close approximation is provided by

$$V = \frac{V_{\max}S_\infty}{k_T + [V_{\max}/(4\pi D)] + S_\infty}. \tag{18.1.4b}$$

Note that this expression has the same form as Equation 18.1.2, with the relevant nutrient concentration now being that in the bulk medium S_∞, and the half-saturation constant being expanded to $k_T + [V_{\max}/(4\pi D)]$.

The overall utility of this approach is that it provides a mechanistic understanding of uptake kinetics in terms of both the cellular features (number, affinity, and handling time of transporters, n_T, k_c, and t_h, respectively), and the additional factors

influencing the magnitude of the diffusive boundary around the cell (embodied in the parameter D). Summarizing from above,

$$V_{\max} = \frac{n_T}{t_h}, \tag{18.1.5a}$$

$$k_S = \frac{1}{t_h}\left(\frac{1}{k_c} + \frac{n_T}{4\pi D}\right), \tag{18.1.5b}$$

which further implies an uptake affinity of

$$\frac{V_{\max}}{k_S} = \frac{(4\pi D)n_T}{(4\pi D/k_c) + n_T}. \tag{18.1.5c}$$

Foundations 18.2. Encounter and capture rates. Ingestion rates are functions of both the rates at which cells physically encounter molecules (or larger prey items) and the subsequent efficiency of particle capture. The preceding theory simply treated the capture rate (per unit substrate concentration) as a fixed constant, but here we go further in mechanistic terms by considering the roles played by the rate of movement of the consumer and its substrate, the size of the cell, and the number of receptors on the surface (transporters) used in capturing the substrate. We first consider the encounter rate, and then the efficiency of capture, the product of which can be viewed as the capture rate k_c.

In Foundations 7.2, it was shown that the rate of encounter between two passively diffusing particles is of the form

$$k_e = 4\pi RD, \tag{18.2.1a}$$

where R is the sum of the radii of the two particles, and D is the sum of their diffusion coefficients. After defining the diffusion coefficients in terms of particle radii, and assuming one particle (in this case, the consumer) is much larger than the other, this leads to

$$k_e \simeq \left(\frac{2k_BT}{3\eta}\right)\left(\frac{r_c}{r_n}\right), \tag{18.2.1b}$$

where k_B is the Boltzmann constant, T is the temperature (in Kelvins), η is the viscosity of the medium, and r_c and r_n are the radii of the consumer cell and the nutrient particle. In this case of passive diffusion, the encounter rate is directly proportional to the width of the consumer cell (here assumed to be a sphere).

Suppose now that the consumer and its prey are capable of swimming at rates well beyond the diffusion rates. Then, each particle type (predator and prey) can be viewed as sweeping through a cylinder at a rate proportional to the square of its radius and the respective swimming velocity (v_c and v_n). Under the assumption of random swimming patterns,

$$k_e = \frac{\pi R^2[(v_c + v_n)^3 - (v_c - v_n)^3]}{6v_cv_n}, \tag{18.2.2a}$$

where R is now taken to be the encounter radius of consumer and substrate, which with a sensory system in the former might exceed the sum $(r_c + r_n)$ (Gerritsen and Strickler 1977). Assuming the prey is a passive nutrient molecule, such that $v_c \gg v_n$, this expression reduces to

$$k_e = \pi R^2 v_c, \tag{18.2.2b}$$

the area of a circle of radius R times the speed of the consumer. Thus, active swimming greatly increases the encounter rate, as this is now proportional to the square of the

radius of the consumer. If turbulence contributes to movement of the consumer and/or substrate, this can be accommodated by addition of an appropriate constant to v_c (Rothschild and Osborn 1988; Evans 1989).

One limitation of these expressions is the assumption of no back-tracking on the part of the consumer, such that the same nutrient concentration is always being encountered, as might be the case if the consumer never changed direction. If, on the other hand, the direction of movement changes stochastically, the consumer will occasionally encounter an already explored patch. In this case, Equation 18.2.1a again applies, but with D redefined to be an effective diffusion coefficient. For example, in the case of run-and-tumble motion (Foundations 16.2), $D = v_c^2\overline{\tau}/(3(1-\overline{c}))$, where $\overline{\tau}$ is the mean time between switching directions, and $\overline{c}$ is the average cosine of the angular change in direction. Equation 18.2.1a then expands to

$$k_e = \frac{4\pi R v_c^2 \overline{\tau}}{3(1-\overline{c})}, \tag{18.2.2c}$$

with the encounter rate again being linear in R (Visser and Kiørboe 2006).

If the consumer cell were 100% efficient at capturing particles upon encounter, the consumption rate would simply be proportional to the encounter rate and the substrate concentration (assuming nonsaturating conditions). However, nutrient uptake generally can only be accomplished when substrate molecules encounter particular receptors on the cell surface. Thus, we must further consider the capture efficiency, an issue first tackled in the pioneering work of Berg and Purcell (1977); additional details can be found in Mitchell (1991, 2002).

The central idea is that conditional upon an encounter, if a particle is not captured by a receptor, it will still diffuse around in the vicinity of the cell for quite some time, providing additional opportunities for proper engagement. Letting r_r be the radius of a receptor, with N_r of these distributed over the surface of the cell, the total area of receptors is $\pi N_r r_r^2$, and the probability that a random encounter does not hit a receptor is one minus the fraction of cell surface occupied by receptors,

$$P_0 = 1 - \frac{N_r r_r^2}{4r_c^2}. \tag{18.2.3}$$

Assuming that each fresh (independent) encounter of the cell starts at approximate distance r_r from the cell surface, the probability that the particle will be captured anew and not lost forever is

$$P_s = \frac{r_c}{r_c + r_r}. \tag{18.2.4}$$

The probability that the particle eventually escapes after a series of encounters is then

$$P_{\text{esc}} = \sum_{i=0}^{\infty} P_0^i P_s^i (1 - P_s) = \frac{1 - P_s}{1 - P_0 P_s}, \tag{18.2.5}$$

which leads to the probability of capture

$$P_{\text{cap}} = 1 - P_{\text{esc}} = \frac{N_r r_r}{4r_c + N_r r_r}. \tag{18.2.6}$$

The rate of successful encounters (the capture rate) is then the product $k_e P_{\text{cap}}$.

This result provides insight into the degree to which a cell membrane needs to be populated by receptors to maintain a high probability of capture of encountered particles. Equation 18.2.6 shows that the probability of capture reaches 50% when the number of receptors per cell is $N_r = 4r_c/r_r$, which would occupy $(\pi r_r^2)(4r_c/r_r)$ of the

total cell surface area ($4\pi r_c^2$), implying a fractional coverage of r_r/r_c. Thus, as receptor diameters are $\ll r_c$, only a small fraction of the cell surface needs to be occupied by receptors to ensure a high capture efficiency.

Foundations 18.3. The cost of osmoregulation. The cytoplasm of cells is often hyperosmotic with respect to the surrounding fluid, causing a tendency for water molecules to enter through the partially permeable cell membrane. Here, we attempt to calculate the energy required to maintain the hyperosmotic states of cells. The pressure difference across a membrane can be computed with the van't Hoff equation,

$$\Delta P = \Delta C \cdot k_B T, \tag{18.3.1}$$

where ΔC is the difference in the concentration of solute molecules across the membrane, k_B is the Boltzmann constant, and T is the temperature (in Kelvins). For most biological temperatures $k_B T \simeq 4.1 \times 10^{-21}$ Joules (1 Joule = 1 kg $\cdot$ M^2 $\cdot$ sec^{-2} = 0.00024 kcal). As an example, the approximate osmolarity of freshwater (summed over all solutes) is 2 mM, or equivalently 2 osmol/M^3. Considering a typical cell with a cytoplasmic osmolarity of 100 osmol/M^3, the concentration difference is 98 osmol/M^3. Multiplying by Avogadro's number of molecules/mol, $\Delta C = 590 \times 10^{23}$ molecules/M^3, and multiplying by $k_B T$ yields $\Delta P = 242,000$ Joules/M^3.

The flow rate across a membrane is equal to the product of the pressure difference, the hydraulic conductivity of the membrane (L_p), and the membrane surface area (A),

$$\Delta F = \Delta P \cdot L_p \cdot A, \tag{18.3.2}$$

where L_p has units of M^4 $\cdot$ sec^{-1} $\cdot$ Joules^{-1} when ΔP is in units of Joules/M^3 and A is in units of M^2, yielding ΔF in units of M^3/sec.

At this point, these formulations may be noninformative to many biologists. However, to understand the challenge that osmotic pressure imposes upon cells, consider that an average freshwater eukaryote has a cell-membrane conductivity $L_p \simeq 7 \times 10^{-15}$ M^4 $\cdot$ sec^{-1} $\cdot$ Joules^{-1} (Raven 1982; Hellebust et al. 1989). Assuming a spherical cell with volume 1000 μm^3, the surface area would be $A = 482$ μm^2, and substitution into Equation 18.3.2 leads to a predicted water intake of $\sim 7 \times 10^4$ μm^3/day, i.e., a daily volumetric intake equal to 70$\times$ the cell volume. To maintain cell homeostasis, this is also the amount of water that must be pumped out of the cell per day.

As the mechanism by which cells expel water is not fully understood, the energy required to maintain osmotic balance remains somewhat uncertain. However, Raven (1982) reasoned out an energetic cost of $\sim 10^{-16}$ mol ATP hydrolyses/μm^3. Using this as an approximation, after multiplying by Avogadro's number, the 1000 μm^3 cell just noted (with a water intake rate of 7×10^4 μm^3/day) would require $\sim 4 \times 10^{12}$ ATP hydrolyses/day for pumping. The daily total maintenance cost for a cell of this size is also $\sim 4 \times 10^{12}$ ATP hydrolyses (Chapter 8). There are a number of uncertainties in these calculations, but assuming they are roughly correct, the implication is that a substantial fraction of cellular maintenance costs in eukaryotic cells derives from the regulation of osmotic balance. For ciliates, it has been estimated that 2 to 40% of total cell energy budgets are associated with contractile-vacuole pumping (increasing with cell volume), with values for *Tetrahymena* and *Paramecium* being in the range of 10 to 15% (Lynch et al. 2022).

Literature Cited

Abascal, F., I. Irisarri, and R. Zardoya. 2014. Diversity and evolution of membrane intrinsic proteins. Biochim. Biophys. Acta 1840: 1468-1481.

Acquisti, C., S. Kumar, and J. J. Elser. 2009. Signatures of nitrogen limitation in the elemental composition of the proteins involved in the metabolic apparatus. Proc. Biol. Sci. 276: 2605-2610.

Alves, R., and M. A. Savageau. 2005. Evidence of selection for low cognate amino acid bias in amino acid biosynthetic enzymes. Mol. Microbiol. 56: 1017-1034.

Armstrong, R. A. 2008. Nutrient uptake rate as a function of cell size and surface transporter density: a Michaelis-like approximation to the model of Pasciak and Gavis. Deep Sea Research Part I: Oceanogr. Res. Papers 55: 1311-1317.

Ashida, H., A. Danchin, and A. Yokota. 2005. Was photosynthetic RuBisCO recruited by acquisitive evolution from RuBisCO-like proteins involved in sulfur metabolism? Res. Microbiol. 156: 611-618.

Badger, M. R., T. J. Andrews, S. M. Whitney, M. Ludwig, D. C. Yellowlees, W. Leggat, and G. D. Price. 1998. The diversity and coevolution of Rubisco, plastids, pyrenoids, and chloroplast-based CO_2-concentrating mechanisms in algae. Can. J. Botany 76: 1052-1071.

Bar-On, Y. M., and R. Milo. 2019. The global mass and average rate of rubisco. Proc. Natl. Acad. Sci. USA 116: 4738-4743.

Baudouin-Cornu, P., Y. Surdin-Kerjan, P. Marlière, and D. Thomas. 2001. Molecular evolution of protein atomic composition. Science 293: 297-300.

Beardall, J., and M. Giordano. 2002. Ecological implications of microalgal and cyanobacterial CO_2 concentrating mechanisms, and their regulation. Func. Plant Biol. 29: 335-347.

Berg, H. C., and E. M. Purcell. 1977. Physics of chemoreception. Biophys. J. 20: 193-219.

Berg, I. A., D. Kockelkorn, W. H. Ramos-Vera, R. F. Say, J. Zarzycki, M. Hügler, B. E. Alber, and G. Fuchs. 2010. Autotrophic carbon fixation in archaea. Nat. Rev. Microbiol. 8: 447-460.

Blount, Z. D., J. E. Barrick, C. J. Davidson, and R. E. Lenski. 2012. Genomic analysis of a key innovation in an experimental *Escherichia coli* population. Nature 489: 513-518.

Bock, C., T. Zollmann, K. A. Lindt, R. Tampé, and R. Abele. 2019. Peptide translocation by the lysosomal ABC transporter TAPL is regulated by coupling efficiency and activation energy. Sci. Rep. 9: 11884.

Bosdriesz, E., M. T. Wortel, J. R. Haanstra, M. J. Wagner, P. de la Torre Cortés, and B. Teusink. 2018. Low affinity uniporter carrier proteins can increase net substrate uptake rate by reducing efflux. Sci. Rep. 8: 5576.

Bouget, F. Y., M. Lefranc, Q. Thommen, B. Pfeuty, J. C. Lozano, P. Schattab, H. Botebo, and V. Vergé. 2014. Transcriptional versus non-transcriptional clocks: a case study in *Ostreococcus*. Mar. Genomics 14: 17-22.

Bouvier, J. W., D. M. Emms, T. Rhodes, J. S. Bolton, A. Brasnett, A. Eddershaw, J. R. Nielsen, A. Unitt, S. M. Whitney, and S. Kelly. 2021. Rubisco adaptation is more limited by phylogenetic constraint than by catalytic trade-off. Mol. Biol. Evol. 38: 2880-2896.

Bragg, J. G., and C. L. Hyder. 2004. Nitrogen versus carbon use in prokaryotic genomes and proteomes. Proc. Biol. Sci. 271 Suppl 5: S374-S377.

Bremer, E., and R. Krämer. 2019. Responses of microorganisms to osmotic stress. Annu. Rev. Microbiol. 73: 313-334.

Brown, N. J., C. A. Newell, S. Stanley, J. E. Chen, A. J. Perrin, K. Kajala, and J. M. Hibberd. 2011. Independent and parallel recruitment of preexisting mechanisms underlying C_4 photosynthesis. Science 331: 1436-1439.

Brunner, M., and M. Merrow. 2008. The green yeast uses its plant-like clock to regulate its animal-like tail. Genes Dev. 22: 825-831.

Buchmann, K., and B. Becker. 2009. The system of contractile vacuoles in the green alga *Mesostigma viride* (Streptophyta). Protist 160: 427-443.

Cardona, T. 2015. A fresh look at the evolution and diversification of photochemical reaction centers. Photosynth. Res. 126: 111-134.

Cardona, T., J. W. Murray, and A. W. Rutherford. 2015. Origin and evolution of water oxidation before the last common ancestor of the cyanobacteria. Mol. Biol. Evol. 32: 1310-1328.

Chakraborty, S., L. T. Nielsen, and K. H. Andersen. 2017. Trophic strategies of unicellular plankton. Am. Nat. 189: E77-E90.

Chen, M., and R. E. Blankenship. 2011. Expanding the solar spectrum used by photosynthesis. Trends Plant Sci. 16: 427-431.

Chew, J., E. Leypunskiy, J. Lin, A. Murugan, and M. J. Rust. 2018. High protein copy number is required to suppress stochasticity in the cyanobacterial circadian clock. Nat. Commun. 9: 3004.

Claessen, D., and J. Errington. 2019. Cell wall deficiency as a coping strategy for stress. Trends Microbiol. 27: 1025-1033.

Collos, Y., A. Vaquer, and P. Souchou. 2005. Acclimation of nitrate uptake by phytoplankton to high substrate levels. J. Phycol. 41: 466-478.

Driessen, A. J., B. P. Rosen, and W. N. Konings. 2000. Diversity of transport mechanisms: common structural principles. Trends Biochem. Sci. 25: 397-401.

Edwards, K. F., M. K. Thomas, C. A. Klausmeier, and E. Litchman. 2012. Allometric scaling and taxonomic variation in nutrient utilization traits and maximum growth rate of phytoplankton. Limnol. Oceanogr. 57: 554-566.

Eelderink-Chen, Z., G. Mazzotta, M. Sturre, J. Bosman, T. Roenneberg, and M. Merrow. 2010. A circadian clock in *Saccharomyces cerevisiae*. Proc. Natl. Acad. Sci. USA 107: 2043-2047.

Eide, D. J. 2012. An "inordinate fondness for transporters" explained? Science Signaling 5: 5.

Erb, T. J., and J. Zarzycki. 2018. A short history of RubisCO: the rise and fall (?) of nature's predominant CO(2) fixing enzyme. Curr. Opin. Biotechnol. 49: 100-107.

Errington, J. 2017. Cell wall-deficient, L-form bacteria in the 21st century: a personal perspective. Biochem. Soc. Trans. 45: 287-295.

Errington, J., K. Mickiewicz, Y. Kawai, and L. J. Wu. 2016. L-form bacteria, chronic diseases and the origins of life. Philos. Trans. R. Soc. Lond. B Biol. Sci. 371: 20150494.

Evans, G. T. 1989. The encounter speed of moving predator and prey. J. Plank. Res. 11: 415-417.

Falkowski, P. G., and J. A. Raven. 2007. Aquatic Photosynthesis. 2nd Ed. Princeton Univ. Press, Princeton, NJ.

Fasani, R. A, and M. A. Savageau. 2014. Evolution of a genome-encoded bias in amino acid biosynthetic pathways is a potential indicator of amino acid dynamics in the environment. Mol. Biol. Evol. 31: 2865-2878.

Feeney, K. A., L. L. Hansen, M. Putker, C. Olivares-Yañez, J. Day, L. J. Eades, L. F. Larrondo, N. P. Hoyle, J. S. O'Neill, and G. van Ooijen. 2016. Daily magnesium fluxes regulate cellular timekeeping and energy balance. Nature 532: 375-379.

Fischer, W. W., J. Hemp, and J. E. Johnson. 2016. Evolution of oxygenic photosynthesis. Annu. Rev. Earth Planetary Sci. 44: 647-683.

Flamholz, A. I., N. Prywes, U. Moran, D. Davidi, Y. M. Bar-On, L. M. Oltrogge, R. Alves, D. Savage, and R. Milo. 2019. Revisiting trade-offs between Rubisco kinetic parameters. Biochemistry 58: 3365-3376.

Folsom, J. P., and R. P. Carlson. 2015. Physiological, biomass elemental composition and proteomic analyses of *Escherichia coli* ammonium-limited chemostat growth, and comparison with iron- and glucose-limited chemostat growth. Microbiology 161: 1659-1670.

Fuchs, G. 2011. Alternative pathways of carbon dioxide fixation: insights into the early evolution of life? Annu. Rev. Microbiol. 65: 631-658.

Galmés, J., P. J. Andralojc, M. V. Kapralov, J. Flexas, A. J. Keys, A. Molins, M. A. Parry, and À. M. Conesa. 2014a. Environmentally driven evolution of Rubisco and improved photosynthesis and growth within the C3 genus *Limonium* (Plumbaginaceae). New Phytol. 203: 989-999.

Galmés, J., M. V. Kapralov, P. J. Andralojc, M. À. Conesa, A. J. Keys, M. A. Parry, and J. Flexas. 2014b. Expanding knowledge of the Rubisco kinetics variability in plant species: environmental and evolutionary trends. Plant Cell. Environ. 37: 1989-2001.

Gerritsen, J., and J. R. Strickler. 1977. Encounter probabilities and community structure in zooplankton: a mathematical model. J. Fish. Res. Bd. Canada 34: 73-82.

Gomez-Fernandez, B. J., E. Garcia-Ruiz, J. Martin-Diaz, P. Gomez de Santos, P. Santos-Moriano, F. J. Plou, A. Ballesteros, M. Garcia, M. Rodriguez, V. A. Risso, et al. 2018. Directed *in vitro* evolution of Precambrian and extant Rubiscos. Sci. Rep. 8: 5532.

Greene, D. N., S. M. Whitney, and I. Matsumura. 2007. Artificially evolved *Synechococcus* PCC6301 Rubisco variants exhibit improvements in folding and catalytic efficiency. Biochem. J. 404: 517-524.

Greganova, E., M. Steinmann, P. Mäser, and N. Fankhauser. 2013. *In silico* ionomics segregates parasitic from free-living eukaryotes. Genome Biol. Evol. 5: 1902-1909.

Grzymski, J. J, and A. M. Dussaq. 2012. The significance of nitrogen cost minimization in proteomes of marine microorganisms. ISME J. 6: 71-80.

Guasto, J. S., R. Rusconi, and R. Stocker. 2012. Fluid mechanics of planktonic microorganisms. Ann. Rev. Fluid Mechanics 44: 373-400.

Gudelj, I., R. E. Beardmore, S. S. Arkin, and R. C. MacLean. 2007. Constraints on microbial metabolism drive evolutionary diversification in homogeneous environments. J. Evol. Biol. 20:

1882-1889.

Günther, T., C. Lampei, and K. J. Schmid. 2013. Mutational bias and gene conversion affect the intraspecific nitrogen stoichiometry of the *Arabidopsis thaliana* transcriptome. Mol. Biol. Evol. 30: 561-568.

Hellebust, J. A., T. Mérida, and I. Ahmad. 1989. Operation of contractile vacuoles in the euryhaline green flagellate *Chlamydomonas pulsatilla* (Chlorophyceae) as a function of salinity. Mar. Biol. 100: 373-379.

Helling, R. B., C. N. Vargas, and J. Adams. 1987. Evolution of *Escherichia coli* during growth in a constant environment. Genetics 116: 349-358.

Hennaut, C., F. Hilger, and M. Grenson. 1970. Space limitation for permease insertion in the cytoplasmic membrane of *Saccharomyces cerevisiae*. Biochem. Biophys. Res. Commun. 39: 666-671.

Heyduk, K., J. J. Moreno-Villena, I. S. Gilman, P. A. Christin, and E. J. Edwards. 2019. The genetics of convergent evolution: insights from plant photosynthesis. Nat. Rev. Genet. 20: 485-493.

Higgins, C. F. 1992. ABC transporters: from microorganisms to man. Annu. Rev. Cell Biol. 8: 67-113.

Hill, J. F., and Govindjee. 2014. The controversy over the minimum quantum requirement for oxygen evolution. Photosynth. Res. 122: 97-112.

Hobson, L.A., and K. P. Guest. 1983. Values of net compensation irradiation and their dependence on photosynthetic efficiency and respiration in marine unicellular algae. Mar. Biol. 74: 1-7.

Holtzendorff, J., F. Partensky, D. Mella, J. F. Lennon, W. R. Hess, and L. Garczarek. 2008. Genome streamlining results in loss of robustness of the circadian clock in the marine cyanobacterium *Prochlorococcus marinus* PCC 9511. J. Biol. Rhythms 23: 187-199.

Hong, C. I., J. Zámborszky, M. Baek, L. Labiscsak, K. Ju, H. Lee, L. F. Larrondo, A. Goity, H. Siong Chong, W. J. Belden, et al. 2014. Circadian rhythms synchronize mitosis in *Neurospora crassa*. Proc. Natl. Acad. Sci. USA 111: 1397-1402.

Itzhak, D. N., S. Tyanova, J, Cox, and G. H. Borner. 2016. Global, quantitative and dynamic mapping of protein subcellular localization. eLife 5: e16950.

Kageyama, H., T. Nishiwaki, M. Nakajima, H. Iwasaki, T. Oyama, and T. Kondo. 2006. Cyanobacterial circadian pacemaker: Kai protein complex dynamics in the KaiC phosphorylation cycle *in vitro*. Mol. Cell. 23: 161-171.

Kapralov, M. V., and D. A. Filatov. 2007. Widespread positive selection in the photosynthetic Rubisco enzyme. BMC Evol. Biol. 7: 73.

Kruckeberg, A. L., L. Ye, J. A. Berden, and K. van Dam. 1999. Functional expression, quantification and cellular localization of the Hxt2 hexose transporter of *Saccharomyces cerevisiae* tagged with the green fluorescent protein. Biochem. J. 339: 299-307.

Lambert, G., J. Chew, and M. J. Rust. 2016. Costs of clock-environment misalignment in individual cyanobacterial cells. Biophys. J. 111: 883-891.

Lear, J. D., Z. R. Wasserman, and W. F. DeGrado. 1988. Synthetic amphiphilic peptide models for protein ion channels. Science 240: 1177-1181.

Levy, S., M. Kafri, M. Carmi, and N. Barkai. 2011. The competitive advantage of a dual-transporter system. Science 334: 1408-1412.

Leypunskiy, E., J. Lin, H. Yoo, U. Lee, A. R. Dinner, and M. J. Rust. 2017. The cyanobacterial circadian clock follows midday *in vivo* and *in vitro*. eLife 6: e23539.

Litchman, E., C. A. Klausmeier, O. M. Schofield, and P. G. Falkowski. 2007. The role of functional traits and tradeoffs in structuring phytoplankton communities: scaling from cellular to ecosystem level. Ecol. Letters 10: 1170-1181.

Lomas, M. W., J. A. Bonachela, S. A. Levin, and A. C. Martiny. 2014. Impact of ocean phytoplankton diversity on phosphate uptake. Proc. Natl. Acad. Sci. USA 111: 17540-17545.

Long, H., W. Sung, S. Kucukyildirim, E. Williams, S. F. Miller, W. Guo, C. Patterson, C. Gregory, C. Strauss, C. Stone, et al. 2017. Evolutionary determinants of genome-wide nucleotide composition. Nature Ecol. Evol. 2: 237-240.

Loukin, S. H., M. M. Kuo, X. L. Zhou, W. J. Haynes, C. Kung, and Y. Saimi. 2005. Microbial K+ channels. J. Gen. Physiol. 125: 521-527.

Lycklama A Nijeholt, J. A., R. Vietrov, G. K. Schuurman-Wolters, and B. Poolman. 2018. Energy coupling efficiency in the Type I ABC transporter GlnPQ. J. Mol. Biol. 430: 853-866.

Lynch, M., and K. Hagner. 2014. Evolutionary meandering of intermolecular interactions along the drift barrier. Proc. Natl. Acad. Sci. USA 112: E30-E38.

Lynch, M., and G. K. Marinov. 2015. The bioenergetic costs of a gene. Proc. Natl. Acad. Sci. USA 112: 15690-15695.

Lynch, M., P. Schavemaker, T. Licknack, and Y. Hao, and A. Pezzano. 2022. Evolutionary bioenergetics of ciliates. J. Euk. Microbiol. 69: e12934.

Lynn, D. H. 1982. Dimensionality and contractile vacuole function in ciliated protozoa. J. Exp. Zool. 223: 219-229.

Lyons, T. W., C. T. Reinhard, and N. J. Planavsky. 2014. The rise of oxygen in Earth's early ocean and atmosphere. Nature 506: 307-315.

Maeda, N., T. Kanai, H. Atomi, and T. Imanaka. 2002. The unique pentagonal structure of an archaeal Rubisco is essential for its high thermostability. J. Biol. Chem. 277: 31656-31662.

Maharjan, R. P., S. Seeto, and T. Ferenci. 2007. Divergence and redundancy of transport and metabolic rate-yield strategies in a single *Escherichia coli* population. J. Bacteriol. 189: 2350-2358.

Marañón, E. 2015. Cell size as a key determinant of phytoplankton metabolism and community structure. Ann. Rev. Mar. Sci. 7: 241-264.

Mazel, D., and P. Marlière. 1989. Adaptive eradication of methionine and cysteine from cyanobacterial light-harvesting proteins. Nature 341: 245-248.

Melis, A. 2009. Solar energy conversion efficiencies in photosynthesis: minimizing the chlorophyll antennae to maximize efficiency. Plant Science 177: 272-280.

Mitchell, J. G. 1991. The influence of cell size on marine bacterial motility and energetics. Microbial Ecol. 22: 227-238.

Mitchell, J. G. 2002. The energetics and scaling of search strategies in bacteria. Amer. Nat. 160:

727-740.

Mofatteh, M., F. Echegaray-Iturra, A. Alamban, F. Dalla Ricca, A. Bakshi, and M. G. Aydogan. 2021. Autonomous clocks that regulate organelle biogenesis, cytoskeletal organization, and intracellular dynamics. eLife 10: e72104.

Morse, D., P. Salois, P. Markovic, and J. W. Hastings. 1995. A nuclear-encoded form II RuBisCO in dinoflagellates. Science 268: 1622-1624.

Mulkidjanian, A. Y., M. Y. Galperin, and E. V. Koonin. 2009. Co-evolution of primordial membranes and membrane proteins. Trends Biochem. Sci. 34: 206-215.

Naftalin, R. J., N. Green, and P. Cunningham. 2007. Lactose permease H^+-lactose symporter: mechanical switch or Brownian ratchet? Biophys. J. 92: 3474-3491.

Nakajima, M., K. Imai, H. Ito, T. Nishiwaki, Y. Murayama, H. Iwasaki, T. Oyama, and T. Kondo. 2005. Reconstitution of circadian oscillation of cyanobacterial KaiC phosphorylation *in vitro*. Science 308: 414-415.

Noordally, Z. B., and A. J. Millar. 2015. Clocks in algae. Biochemistry 54: 171-183.

O'Neill, J. S., G. van Ooijen, L. E. Dixon, C. Troein, F. Corellou, F. Y. Bouget, A. B. Reddy, and A. J. Millar. 2011. Circadian rhythms persist without transcription in a eukaryote. Nature 469: 554-558.

Oren, A. 1999. Bioenergetic aspects of halophilism. Microbiol. Mol. Biol. Rev. 63: 334-348.

Partch, C. L., C. B. Green, and J. S. Takahashi. 2014. Molecular architecture of the mammalian circadian clock. Trends Cell Biol. 24: 90-99.

Pasciak, W. J., and J. Gavis. 1974. Transport limitation of nutrient uptake in phytoplankton. Limnol. Oceanogr. 19: 881-888.

Pattanayak, G. K., G. Lambert, K. Bernat, and M. J. Rust. 2015. Controlling the cyanobacterial clock by synthetically rewiring metabolism. Cell Rep. 13: 2362-2367.

Patzlaff, J. S., T. van der Heide, and B. Poolman. 2003. The ATP/substrate stoichiometry of the ATP-binding cassette (ABC) transporter OpuA. J. Biol. Chem. 278: 29546-29551.

Phillips, R., and R. Milo. 2009. A feeling for the numbers in biology. Proc. Natl. Acad. Sci. USA 106: 21465-21471.

Phong, C., J. S. Markson, C. M. Wilhoite, and M. J. Rust. 2013. Robust and tunable circadian rhythms from differentially sensitive catalytic domains. Proc. Natl. Acad. Sci. USA 110: 1124-1129.

Pittayakanchit, W., Z. Lu, J. Chew, M. J. Rust, and A. Murugan. 2018. Biophysical clocks face a trade-off between internal and external noise resistance. eLife 7: e37624.

Pohorille, A., K. Schweighofer, and M. A. Wilson. 2005. The origin and early evolution of membrane channels. Astrobiology 5: 1-17.

Poudel, S., D. H. Pike, H. Raanan, J. A. Mancini, V. Nanda, R. E. M. Rickaby, and P. G. Falkowski. 2020. Biophysical analysis of the structural evolution of substrate specificity in RuBisCO. Proc. Natl. Acad. Sci. USA 117: 30451-30457.

Purcell, E. M. 1977. Life at low Reynolds number. Amer. J. Physics 45: 3.

Raven, J. A. 1982. The energetics of freshwater algae: energy requirements for biosynthesis and volume regulation. New Phytol. 92: 1-20.

Raven, J. A. 2009. Contributions of anoxygenic and oxygenic phototrophy and chemolithotrophy to carbon and oxygen fluxes in aquatic environments. Aquatic Microb. Ecol. 56: 177-192

Raven, J. A. 2017. The possible roles of algae in restricting the increase in atmospheric CO_2 and global temperature. European J. Phycol. 52: 506-522.

Raven, J. A., J. Beardall, and P. Sánchez-Baracaldo. 2017. The possible evolution and future of CO_2-concentrating mechanisms. J. Exp. Bot. 68: 3701-3716.

Raven, J. A., and M. A. Doblin. 2014. Active water transport in unicellular algae: where, why, and how. J. Exp. Bot. 65: 6279-6292.

Roenneberg, T., and M. Merrow. 2001. Circadian systems: different levels of complexity. Philos. Trans. R. Soc. Lond. B Biol. Sci. 356: 1687-1696.

Rothschild, B. J., and T. R. Osborn. 1988. Small-scale turbulence and plankton contact rates. J. Plank. Res. 10: 465-474.

Rozhoňová, H., and J. L. Payne. 2021. Little evidence the standard genetic code is optimized for resource conservation. Mol. Biol. Evol. 38: 5127-5133.

Samani, P., and G. Bell. 2016. Experimental evolution of the grain of metabolic specialization in yeast. Ecol. Evol. 6: 3912-3922.

Sancar, A. 2008. The intelligent clock and the Rube Goldberg clock. Nat. Struct . Mol. Biol. 15: 23-24.

Sartor, F., Z. Eelderink-Chen, B. Aronson, J. Bosman, L. E. Hibbert, A. N. Dodd, Á. T. Kovács, and M. Merrow. 2019. Are there circadian clocks in non-photosynthetic bacteria? Biology (Basel) 8: E41.

Savir, Y., E. Noor, R. Milo, and T. Tlusty. 2010. Cross-species analysis traces adaptation of Rubisco toward optimality in a low-dimensional landscape. Proc. Natl. Acad. Sci. USA 107: 3475-3480.

Schulz, L., Z. Guo, J. Zarzycki, W. Steinchen, J. M. Schuller, T. Heimerl, S. Prinz, O. Mueller-Cajar, T. J. Erb, and G. K. A. Hochberg. 2022. Evolution of increased complexity and specificity at the dawn of form I Rubiscos. Science 378: 155-160.

Shenhav, L., and D. Zeevi. 2020. Resource conservation manifests in the genetic code. Science 370: 683-687.

Shih, P. M. 2015. Photosynthesis and early Earth. Curr. Biol. 25: R855-R859.

Shih, P. M., A. Occhialini, J. C. Cameron, P. J. Andralojc, M. A. Parry, and C. A. Kerfeld. 2016. Biochemical characterization of predicted Precambrian RuBisCO. Nat. Commun. 7: 10382.

Shih, P. M., L. M. Ward, and W. W. Fischer. 2017. Evolution of the 3-hydroxypropionate bicycle and recent transfer of anoxygenic photosynthesis into the Chloroflexi. Proc. Natl. Acad. Sci. USA 114: 10749-10754.

Short, M. B., C. A. Solari, S. Ganguly, T. R. Powers, J. O. Kessler, and R. E. Goldstein. 2006. Flows driven by flagella of multicellular organisms enhance long-range molecular transport. Proc. Natl. Acad. Sci. USA 103: 8315-8319.

Solari, C. A., K. Drescher, S. Ganguly, J. O. Kessler, R. E. Michod, and R. E. Goldstein. 2011. Flagellar phenotypic plasticity in volvocalean algae correlates with Péclet number. J. R. Soc. Interface 8: 1409-1417.

Spreitzer, R. J., and M. E. Salvucci. 2002. Rubisco: structure, regulatory interactions, and possibilities for a better enzyme. Annu. Rev. Plant Biol. 53: 449-475.

Stefan, E., S. Hofmann, and R. Tampé. 2020. A single power stroke by ATP binding drives substrate translocation in a heterodimeric ABC transporter. eLife 9: e55943.

Stevens, T. J., and I. T. Arkin. 2000. Do more complex organisms have a greater proportion of membrane proteins in their genomes? Proteins 39: 417-420.

Stroppolo, M. E., M. Falconi, A. M. Caccuri, and A. Desideri. 2001. Superefficient enzymes. Cell. Mol. Life Sci. 58: 1451-1460.

Tcherkez, G. G., G. D. Farquhar, and T. J. Andrews. 2006. Despite slow catalysis and confused substrate specificity, all ribulose bisphosphate carboxylases may be nearly perfectly optimized. Proc. Natl. Acad. Sci. USA 103: 7246-7251.

Terauchi, K., Y. Kitayama, T. Nishiwaki, K. Miwa, Y. Murayama, T. Oyama, and T. Kondo. 2007. ATPase activity of KaiC determines the basic timing for circadian clock of cyanobacteria. Proc. Natl. Acad. Sci. USA 104: 16377-16381.

Thauer, R. K. 2007. A fifth pathway of carbon fixation. Science 318: 1732-1733.

Tilman, G. D. 1982. Resource Competition and Community Structure. Monogr. Pop. Biol. 17. Princeton Univ. Press, Princeton, NJ.

Tortell, P. D. 2000. Evolutionary and ecological perspectives on carbon acquisition in phytoplankton. 45: 744-750.

Uemura, K., Anwaruzzaman, S. Miyachi, and A. Yokota. 1997. Ribulose-1,5-bisphosphate carboxylase/oxygenase from thermophilic red algae with a strong specificity for CO_2 fixation. Biochem. Biophys. Res. Commun. 233: 568-571.

van Ooijen, G., L. E. Dixon, C. Troein, and A. J. Millar. 2011. Proteasome function is required for biological timing throughout the twenty-four hour cycle. Curr. Biol. 21: 869-875.

Visser, A. W., and T. Kiørboe. 2006. Plankton motility patterns and encounter rates. Oecologia 148: 538-546.

Wallin, E., and G. von Heijne. 1998. Genome-wide analysis of integral membrane proteins from eubacterial, archaean, and eukaryotic organisms. Protein Sci. 7: 1029-1038.

Waygood, E. B., and T. Steeves. 1980. Enzyme I of the phosphoenolpyruvate: sugar phosphotransferase system of *Escherichia coli*. Purification to homogeneity and some properties. Can. J. Biochem. 58: 40-48.

Wilson, R. H., E. Martin-Avila, C. Conlan, and S. M. Whitney. 2018. An improved *Escherichia coli* screen for Rubisco identifies a protein-protein interface that can enhance CO_2-fixation kinetics. J. Biol. Chem. 293: 18-27.

Woese, C. R. 1987. Bacterial evolution. Microbiol. Rev. 51: 221-271.

Woese, C. R, B. A. Debrunner-Vossbrinck, H. Oyaizu, E. Stackebrandt, and W. Ludwig. 1985. Gram-positive bacteria: possible photosynthetic ancestry. Science 229: 762-765.

Wykoff, D. D., A. H. Rizvi, J. M. Raser, B. Margolin, and E. K. O'Shea. 2007. Positive feedback regulates switching of phosphate transporters in *S. cerevisiae.* Mol. Cell. 27: 1005-1013.

Xu, H., and J. Zhang. 2021. Is the genetic code optimized for resource conservation? Mol. Biol. Evol. Mol. Biol. Evol. 38: 5122-5126.

Ye, L., J. A. Berden, K. van Dam, and A. L. Kruckeberg. 2001. Expression and activity of the Hxt7 high-affinity hexose transporter of *Saccharomyces cerevisiae.* Yeast 18: 1257-1267.

Young, J. N., R. E. Rickaby, M. V. Kapralov, and D. A. Filatov. 2012. Adaptive signals in algal Rubisco reveal a history of ancient atmospheric carbon dioxide. Philos. Trans. R. Soc. Lond. B Biol. Sci. 367: 483-492.

Zehr, J. P., J. S. Weitz, and I. Joint. 2017. How microbes survive in the open ocean. Science 357: 646-647.

Zhou, Y., and S. Whitney. 2019. Directed evolution of an improved Rubisco; *in vitro* analyses to decipher fact from fiction. Int. J. Mol. Sci. 20: 5019.

Figure 18.1. A structural explanation for the use of dual high/low-affinity transporters for nutrient uptake. **Left)** Transporters can be bidirectional, in the sense that they can bind to substrates on both sides of the membrane. In that case, when nutrient concentrations are high internally and externally, rates of influx will be nearly equal to those of efflux. However, low affinity transporters require higher concentrations to become saturated, and therefore maintain larger differences between influx and eflux rates at high nutrient concentrations. **Right)** Net influx rates for transporters with different affinities (k_S, x axis) are given for three substrate concentrations (solid lines) and assuming constant $V_{\max}$. Low k_S (half-saturation constant) implies high affinity for the substrate. Net influx is low when k_S is low because saturation occurs at very low substrate concentrations, and the high affinity leads to near equal levels of binding on both sides of the membrane. On the other hand, with very high k_S, although there is little competitive binding, the overall influx rate is low simply because of the low absolute affinity on the external side of the membrane. Overall rates of influx increase with nutrient concentration regardless of k_S, but the optimum k_S shifts to the right (meaning that the optimum affinity is lowered) with higher concentrations. The dashed lines show the behavior that would occur with purely Michaelis-Menten uptake dynamics – in this case, the optimal k_S is always zero, as there is no competitive binding on the inside of the membrane. Derivations and other details can be found in Bosdriesz et al. (2018).

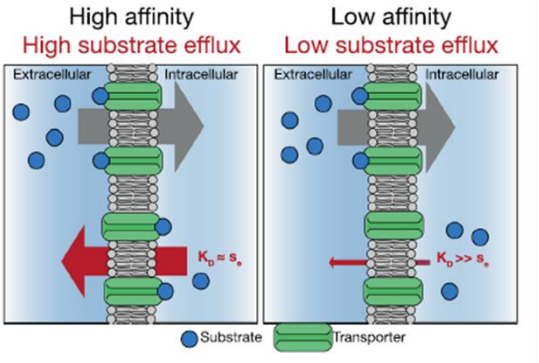

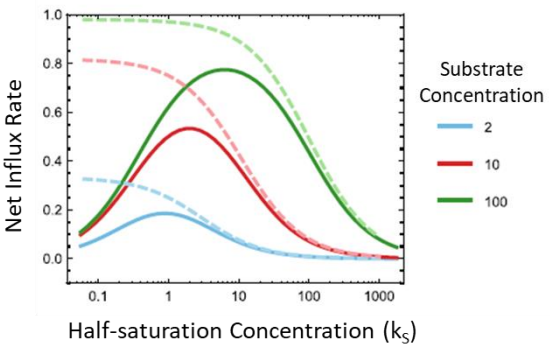

Figure 18.2. The historical record of the Earth's atmospheric CO_2 and O_2 concentrations, given as a crude idealization of patterns outlined in Shih (2015) and Raven (2017). Note that the vertical axis is on a logarithmic scale.

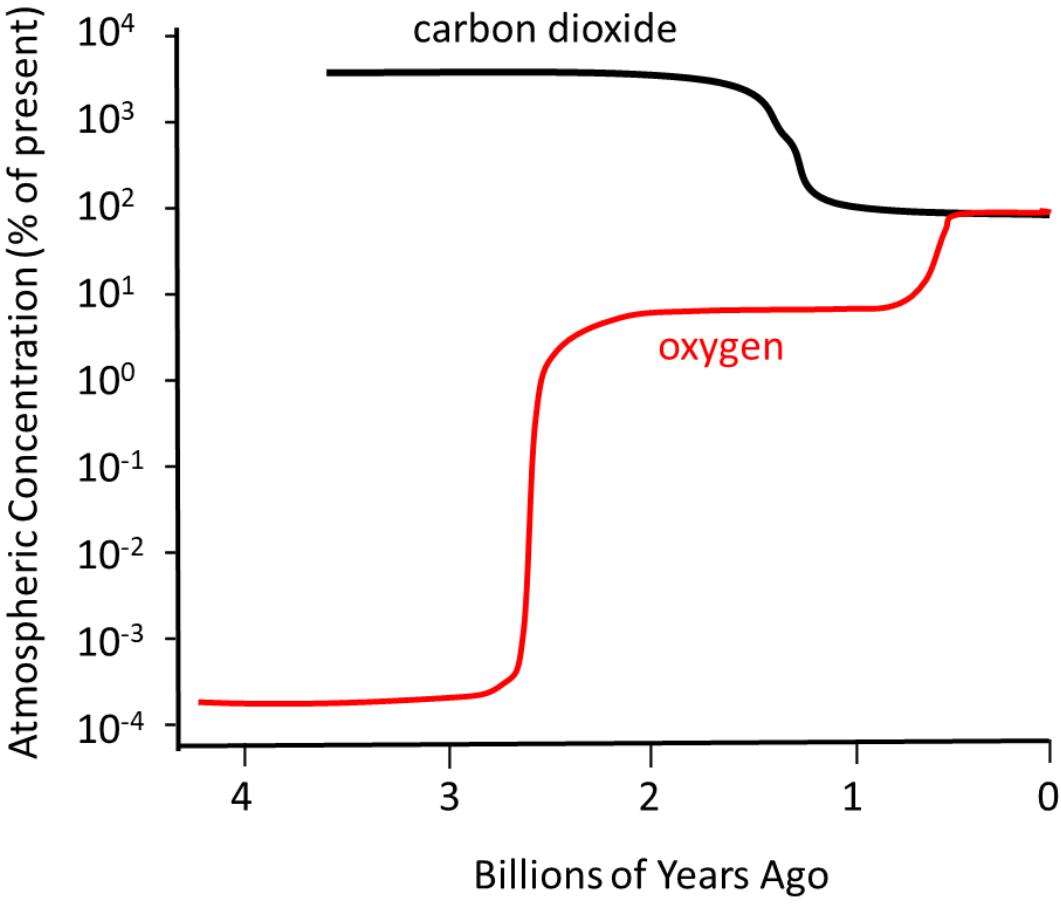

Figure 18.3. Some compatible solutes commonly deployed in osmotic regulation in prokaryotes and eukaryotes, and the biosynthetic costs per molecule (in parentheses, and in units of ATP hydrolyses). Taken from Oren (1999; his Figure 2), with the costs modified to be compatible with the recipes outlined in Foundations 17.2.

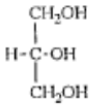

Glycerol

(20)

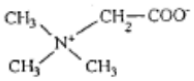

Glycine betaine

(27)

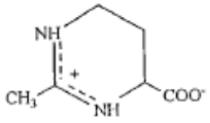

Ectoine

(40)

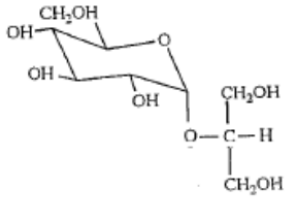

Glucosylglycerol

(53)

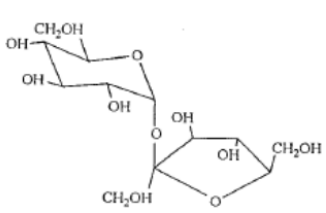

Sucrose

(66)

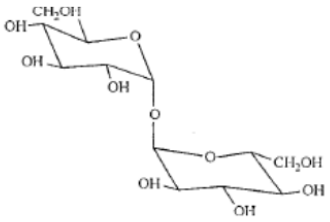

Trehalose

(66)

Figure 18.4. The molecular network for the circadian clock in the cyanobacterium *Synechococcus*. **Left)** Hexameric KaiC is autophosphorylated in the presence of KaiA (right), until it is joined by KaiB (left), which encourages dephosphorylation. Driven by ATP, this cyclical pattern results in stable oscillations. From Phong et al. (2013). **Right)** A simplified view of the vertebrate molecular clock. The heterodimeric transcription factor Clock/Bmal1 activates transcription of the Per and Cry genes, the mRNAs of which are translated in the cytoplasm. The proteins of the latter two genes then heterodimerize, return to the nucleus, and suppress their own expression. The kinetics lead to stable 24-hour cycles. From Partch et al. (2014).